Title

Extensive, transient, and long-lasting gene regulation in a song-controlling brain area during testosterone-induced song development in adult female canaries

Authors

Meng-Ching Ko[1*], Carolina Frankl-Vilches[1], Antje Bakker[1], Nina Sohnius-Wilhelmi[1], Pepe Alcami[1,2], Manfred Gahr[1]

Affiliations

[1] Department of Behavioural Neurobiology, Max Planck Institute for Biological Intelligence, Seewiesen, 82319, Germany.

[2] Division of Neurobiology, Faculty of Biology, Ludwig-Maximilians-University Munich, Grosshaderner Strasse 2, 82152 Planegg-Martinsried, Germany.

* Corresponding authors, E-mail: mengching.ko@bi.mpg.de; carolina.frankl@bi.mpg.de; manfred.gahr@bi.mpg.de

Abstract

Like other canary reproductive behaviors, song production occurs seasonally and can be triggered by gonadal hormones. Adult female canaries treated with testosterone sing first songs after four days and progressively develop towards typical canary song structure over several weeks, a behavior that females otherwise rarely or never show. We compared gene regulatory networks in the song-controlling brain area HVC after 1 hour (h), 3 h, 8 h, 3 days (d), 7d, and 14d testosterone treatment with placebo-treated control females, paralleling HVC and song development. Rapid onset (1 h or less) of extensive transcriptional changes (2,700 genes) preceded the onset of song production by four days. The highest level of differential gene expression occurred at 14 days when song structure was most elaborate and song activity was highest. The transcriptomes changed massively several times during the two-week of song production. A total of 9,710 genes were differentially expressed, corresponding to about 60% of the known protein-coding genes of the canary genome. Most (99%) of the differentially expressed genes were regulated only at specific stages. The differentially

expressed genes were associated with diverse biological functions, the cellular level occurring early and the nervous system level occurring primarily after prolonged testosterone treatment. Thus, the development of adult songs stimulated by testosterone results in widespread transcriptional changes in the HVC, potentially affecting a majority of neuronal subpopulations rather than altering only specific cellular components. Parallel gene regulation directly by androgen and estrogen receptors, potentially amplified by co-expressed transcription factors that are themselves steroid receptor regulated, leads to substantial transcriptomic and neural changes in specific behavior-controlling brain areas, resulting in the gradual seasonal occurrence of singing behavior.

Introduction

Adult socio-sexual behaviors in vertebrates, such as seasonal changes in brain areas' sensitivities to gonadal hormones (Quispe et al., 2015; Riters et al., 2000; Schlinger et al., 1984; Sharp et al., 1986; Watts, 2020), are crucial for the occurrence of reproductive behaviors. These behaviors are regulated by androgens and estrogens, which fluctuate in response to environmental conditions (Ball and Balthazart, 2002; Guh et al., 2019; Weems et al., 2015). Seasonal changes in behavior and underlying sensory and motor brain functions are attributed to gonadal hormone-dependent activation of existing neural circuits and, in some cases, altered neural circuit configurations (Celec et al., 2015; Forlano et al., 2015; Jennings and de Lecea, 2020; Migaud et al., 2015; Schwartz and Andrews, 2013; Zornik and Kelley, 2011). A prominent example is the seasonal singing of some songbird species, which coincides with a seasonal change of morphology of song controlling brain regions (Alliende et al., 2017; Apfelbeck et al., 2012; Ball et al., 2004; de Bournonville et al., 2021; Gahr, 2004; Gahr, 2020; Nottebohm, 1981).

Androgens and estrogens bind to their respective receptors (androgen receptor (AR), estrogen receptor α (ESR1), estrogen receptor ß (ESR2)), initiating transcription of gene cascades or activating intracellular second messenger pathways through non-genomic actions (Celec et al., 2015;

Fuentes and Silveyra, 2019). During differentiation, androgens and estrogens are thought to activate tissue-specific hub genes, initiating cascades that regulate numerous genes and determine tissue function (Pihlajamaa et al., 2015). In adults, while gonadal hormones may affect several regions of a neural circuit, the impacted gene cascades within a specific brain region seem limited (Bao et al., 2019; Peterson et al., 2013; Schwartz et al., 2013; Zhang et al., 2016; Zhao et al., 2021). Unraveling the complex interplay between hormones, gene expression, brain structure, and behavior is challenging, particularly when investigating the influence of hormone-triggered cascades on behaviors that emerge slowly over time, such as the seasonal singing of canaries (Nottebohm et al., 1986; Voigt and Leitner, 2008).

Singing behavior is a complex process involving intensive integration of sensory inputs and motor outputs (Wild, 2004). Songbirds use songs in reproductive contexts such as mate attraction (Byers et al., 2010; Drăgănoiu et al., 2002), pair bond formation (Wickler and Seibt, 1980), competitions with other males (Alcami et al., 2021), and territorial defense (Catchpole and Slater, 2018; Snijders et al., 2017). In many North temperate species, sexually motivated singing behavior is typically limited to males and is sensitive to testosterone and its androgenic and estrogenic metabolites (Gahr, 2014). In some species, females can sing in a sexual context, yet they also sing regularly in a non-breeding context (Gahr, 2020; Riebel et al., 2019). Nevertheless, in adult males and females of most bird species, testosterone treatment increases the singing rates and/or alters species-specific song patterns, even in cases where the function of female singing remains unclear (Dittrich et al., 2014; Gahr, 2020; Hausberger et al., 1995).

The neural song control system of songbirds (Nottebohm et al., 1976; Wild, 2004) is a target of testosterone due to the abundant expression of androgen and estrogen receptors (Gahr, 1990b; Johnson and Bottjer, 1995; Metzdorf et al., 1999). The premotor forebrain nucleus HVC, a sensorimotor integration center of the song system (Hahnloser et al., 2002; Yu and Margoliash, 1996), controls the temporal pattern of singing (Hahnloser et al., 2002; Long and Fee, 2008). As the

only song control nucleus expressing both androgen and estrogen receptors (Frankl-Vilches and Gahr, 2017; Gahr, 2001), the HVC is likely subject to extensive hormonal regulation at various organizational levels. Testosterone has been shown to induce angiogenesis in adult female canaries' HVC within a week, mediated by 17β-estradiol (Louissaint et al., 2002), promote gap junction formation (Gahr and Garcia-Segura, 1996), and trigger spine pruning in HVC neurons (Vellema et al., 2019). While a handful of studies documented transcriptomic changes in songbird brains after several weeks of testosterone treatment (Dittrich et al., 2014; Frankl-Vilches et al., 2015; Larson et al., 2015; Peterson et al., 2013; Thompson et al., 2012), the transcriptomic effects at the onset of testosterone-driven singing and the progression of gene expression cascades associated with anatomical changes in the song control system and the development of singing behavior remain unexplored.

Female canaries (*Serinus canaria*) are typically non-singers, with their spontaneous songs displaying less complexity than their male counterparts (Hartley et al., 1997; Herrick and Harris, 1957; Ko et al., 2020; Pesch and Güttinger, 1985). Despite their infrequent singing, these females possess the necessary underlying circuitry that can be activated by testosterone. Following testosterone treatment, these females start to produce simple songs, which gradually evolve in structure over weeks—paralleling the seasonal progression of male singing (Hartog et al., 2009; Ko et al., 2020; Shoemaker, 1939; Vallet et al., 1996; Vellema et al., 2019). Moreover, testosterone induces the differentiation of song control-related brain nuclei in adult female canaries, a critical step for song development (Fusani et al., 2003; Madison et al., 2015; Nottebohm, 1980). In this study, we focus on these testosterone-treated female canaries as a model for adult behavioral development rather than a model for male canaries. This unique model allows us to examine transcriptional cascades in parallel with the differentiation of the song control system and the progression of song development, without the confounding impact of fluctuating testosterone levels seen in males, which often results in considerable individual differences in the non-reproductive season baseline singing

behavior. This approach is backed by the observation that the HVC transcriptomes of testosterone-implanted singing female canaries are distinct from those of singing males (Ko et al., 2021).

Here, we investigate the short- and long-term responses of HVC gene expression following testosterone treatment in adult female canaries. We administered testosterone over six time periods (1 hour (h) [T1h], 3 h [T3h], 8 h [T8h], 3 days (d) [T3d], 7 d [T7d], and 14 d [T14d]; Fig. 1A-B and Table 1) and monitored their vocal activity. We quantified gene expression and correlated the transcriptomic data with neuroanatomical and behavioral measurements from the treated birds to identify the key molecular players in testosterone-driven song development.

Contrary to our expectation that testosterone would initially regulate a small number of hub-genes and gradually recruit more over time, our results reveal that testosterone had an immediate and significant impact on HVC gene expression with dynamic patterns over time. After an initial swift transcriptional change within 1 hour, affecting 2,652 genes, differential gene expression continued to evolve dynamically and surged after 14 days of testosterone treatment, altering the expression of 7,702 genes, including 730 transcription factors. Our study sheds light on the progression of cellular and network-level events in the HVC essential for initiating and developing singing behavior.

Results

We selected non-singing females to obtain a homogenous baseline for testosterone-induced song development in all experimental animals and observed song activity after hormone implantation to determine the timing of testosterone-induced song development (Fig. 1). After testosterone implantation, birds in groups T1h, T3h, T8h, and T3d either called or remained silent and did not sing, while five of six birds in group T7d and all birds in group T14d sang (Figure 1 – Figure supplement 1 and Supplementary File 1). On average, the first recognizable subsongs, which are unstructured and low-amplitude vocalizations consisting of three or more syllables, were uttered 4.1 ± 1.6 (mean ± SD) days after implantation. This aligns with previous reports (Vellema et al., 2019)

and is comparable to the observation that male canaries begin singing after four days in the nonbreeding season when implanted with testosterone (Sartor et al., 2005). One female in the T14 group sang just one day after testosterone treatment. Singing activity increased significantly after day 2 and day 10 of testosterone treatment with no statistical difference in singing activity between day 2 to day 9 (Fig. 1C, Supplementary File 2, and Supplementary File 3).

Testosterone-induced progressive song development.

At the onset of song development, the songs displayed substantial inter- and intra-individual variability (Figure 1 – Figure supplement 2 and Supplementary File 1). Testosterone significantly increased the song lengths daily until day 7 and continued to increase them from day 11 onwards (Fig. 1D, Supplementary File 2, and Supplementary File 3). Similarly, the number of syllables per song also increased daily after implantation (Fig. 1E). Testosterone implantation significantly increased syllable repetition rate in two steps: first on day 2 and then on day 9 (Fig. 1F). The maximum syllable repetition rate of all songs was 26 Hz, consistent with a previous study (Fusani et al., 2003).

Testosterone increased HVC volume after two weeks.

Testosterone increased HVC volume after two weeks: HVC volumes were significantly greater in T14d birds compared to controls (Fig. 1G, CON: 0.103 ± 0.040 mm^3 (mean ± SD); T14d: 0.253 ± 0.087 mm3, Kruskal-Wallis followed by Dunn post hoc test, χ^2 = 16.15, df = 6, Holm-adjusted P-value = 0.013). The HVC volumes of T7d were not significantly different from those of controls (T7d: 0.146 ± 0.073 mm3, Holm-adjusted P-value = 1) and were not different from those of T14d due to the wide variation in HVC volumes of T7d (Holm-adjusted P-value = 0.69). Testosterone-treated birds did not significantly differ from controls in terms of body weight, brain weight, and oviduct weight (Figure 1 – Figure supplement 4A-C). HVC volumes normalized with respect to

brain weight yielded similar results as those without normalization (Kruskal-Wallis test, χ^2 = 17.32, df = 6, P-value = 0.0082, Figure 1 – Figure supplement 4D). The HVC development observed is consistent with previous findings that systemic administration of testosterone results in detectable HVCs in female canaries (Cornez et al., 2020; Fusani et al., 2003; Hartog et al., 2009; Madison et al., 2015; Nottebohm, 1980; Rasika et al., 1994).

Testosterone dramatically altered HVC transcriptomes.

To investigate the effect of testosterone on gene regulation in the HVC, we performed microarray analyses and examined the different gene expression profiles of the six testosterone-treated groups compared with controls. We used microarrays for transcriptome analysis to cope with the small amounts of mRNA that is available from the HVCs of an individual female. The effect of testosterone on transcription was evident as early as 1 hour after implantation (T1h, Fig. 2A), when plasma androgen levels were significantly elevated (Fig. 1B; see Methods). The expression levels of 2,652 genes were significantly different between T1h and controls; 1,539 genes were upregulated and 1,113 were downregulated, including 141 up-regulated transcription factors (TFs) and 80 down-regulated TFs (Fig. 2A and Supplementary File 4). The number of differentially expressed genes fluctuated during testosterone treatment and increased dramatically after 14 days (T14d, Fig. 2A). At 14 days, 5,632 genes were upregulated and 2,070 downregulated, including 525 upregulated and 205 downregulated TFs. These 7,702 genes represent 49% of all currently known protein-coding genes in the canary genome (Frankl-Vilches et al., 2015). Overall, testosterone treatment affected the expression of 9,710 genes across all time points combined, corresponding to approximately 60% of all canary protein-coding genes (Frankl-Vilches et al., 2015).

The vast majority of testosterone-induced genes were only transiently affected.

To gain insight into the temporal dynamics of gene expression altered by testosterone, we classified the differentially expressed genes into four classes: 1) constantly upregulated (at all six time points), 2) constantly downregulated, 3) dynamically regulated genes that the direction of regulation varied between time points, and 4) transiently regulated genes with altered expression at least at one but not all time points (Fig. 2B).

Contrary to our expectation that testosterone would initially regulate a small number of genes upon implantation and gradually influence more genes over time, we observed a rapid and massive impact characterized by a dynamic, nonlinear pattern, where the number of differentially expressed genes does not consistently increase over time but instead displays dynamic fluctuations. The majority of genes differentially expressed after testosterone treatment were transiently regulated genes (9,557 genes), whereas the constant-regulated classes contained only about 50 genes each (Fig. 2B). We further analyzed the transient category by the number of time points a gene was differentially regulated and found that over 50% of these genes were differentially regulated at just one time point (Figure 2 – Figure supplement 1).

Considering the moderate sample sizes of our study, we conducted a power analysis for each differentially expressed gene. The genes with power ≥ 0.8 were then categorized according to the temporal regulation patterns as described above. We found 93% of them (9025 out of 9710) had a power ≥ 0.8. This further analysis yielded 29 consistently upregulated, 41 consistently downregulated, 39 dynamically regulated, and 8916 transiently regulated genes.

Constantly upregulated genes included pleiotropic genes such as the transcription factors *FLII* (FLII actin remodeling protein) and *NOTCH1* (notch receptor 1), which are associated with a variety of cellular processes like morphogenesis of anatomical structures (Limbourg et al., 2005) (Supplementary File 5). Constantly downregulated genes included genes associated with apoptosis,

such as *CASP8AP2* (caspase 8-associated protein 2) and *MAPK14* (mitogen-activated protein kinase 14) (Jia et al., 2009) (Supplementary File 5).

Parallel direct and indirect regulation of many genes by nuclear steroid receptors.

To evaluate the possibility of widespread parallel regulation of the expression of the numerous testosterone-influenced genes by the nuclear gonadal steroid receptors (AR, ESR1, and ESR2), we screened the promoter sequences of the upregulated genes for androgen and estrogen response elements (AREs and EREs, respectively) using the Genomatix-overrepresented TFBS tool. If many promoter sequences of testosterone-regulated genes contained AREs or EREs, nuclear steroid receptors could directly regulate these genes in parallel and rapidly cause extensive changes in the HVC transcriptome. Indeed, both AREs (V$ARE.04) and EREs (V$ER.02, V$ER.03, V$ER.04, and V$ESR2.01) were overrepresented in the promoter sequences of genes that were upregulated within 1 hour of testosterone treatment (Figure 2 - Figure Supplement 2A and Supplementary File 6), which concerned 83.7 % of 962 differentially expressed genes with available promoter sequences (Figure 2 - Figure Supplement 2B). AREs were identified in 45.9% (442), ERE in 7.4% (71) and both ARE and ERE in 30.4% (292) of the promoter sequences of differentially expressed genes. In addition, approximately 9% of the genes upregulated in T1h are transcription factors (141 genes, Fig. 2A); the MatInspector tool of the Genomatix software suite identified AREs and/or EREs in the 31 promoters of the 38 transcription factors whose promoter sequences we were able to obtain (see Supplementary File 7).

After 14 days, when differential gene expression increased massively, the number of differentially transcribed transcription factors was much higher in T14d transcriptomes compared to all other time points (Fig. 2A). Overall, however, the frequency of genes with ARE (48.2%), ERE (7.6%), or both (26.3%) (total 82.1%) among 2,941 promoter-sequence-available differentially expressed genes in T14d-HVCs was similar to that in T1d-HVCs (Figure 2 - Figure Supplement 2C). Therefore, testosterone-regulated hub genes such as transcription factor SP8 (see below), in addition

to androgen and estrogen receptors, may have contributed to strongly increased transcriptional regulation in the HVC at 14 days of song development.

Testosterone affected steroid homeostasis and steroid receptor expression in the HVC. Testosterone can be converted by aromatase (CYP19A1) to the major estrogen 17β-estradiol, by 5α-reductase (SRD5A2) to the active androgen 5α-dihydrotestosterone (5α-DHT), or by 5β-reductase (AKR1D1) to the inactive androgen 5β-dihydrotestosterone (5β-DHT) (Michels and Hoppe, 2008). The active forms of androgens and estrogens can trigger transcription via nuclear androgen and estrogen receptors.

One hour after implantation, the HVC cells appear to act to lower local testosterone and estradiol levels. For example, *AKR1D*1 was upregulated, potentially reducing active androgen levels by promoting the conversion of testosterone to inactive 5β-DHT (Fig. 3A). In addition, upregulation of UDP-glucuronosyltransferase 1A (*UGT1A1* and *UGT1A9*) could decrease the toxicity of 17β-estradiol through conjugation of hydrophilic glucuronides (Guillemette, 2003; Ouzzine et al., 2014). In contrast, the HVC appears to have adjusted to elevated testosterone levels eight hours after implantation: *AKR1D1* and *UGT1A1* were downregulated again, and *SRD5A2* was upregulated instead (Fig. 2E, 2F, 3A, and Figure 3 – Figure supplement 1). In addition, *ESR1* (estrogen receptor α) was now upregulated.

After two weeks of treatment, many genes encoding enzymes involved in steroidogenesis and steroid activity were up-regulated, including *HSD3B2*, *CYP17A1*, *SRD5A2*, *CYP19A1*, *ARK1D1* (except for the down-regulation of *HSD17B12*), the nuclear steroid receptors (*AR* and *ESR2*) as well as the membrane-associated androgen receptor *GPRC6A* (Pi et al., 2010) (Fig. 3A and Figure 3 – Figure supplement 1). The up-regulation of many steroidogenesis enzymes and receptors suggests potentially active biosynthesis of various steroidogenesis metabolites capable of triggering hormone signaling cascades. This might contribute to the high number of differentially expressed genes at T14d.

These changes in mRNA expression are indicative of potential changes in steroid sensitivity in the HVC, which could affect the neural response to steroids. However, we acknowledge that isoform differences of these transcribed enzymes may influence steroid metabolism, and further studies are necessary to confirm our findings and elucidate the mechanisms underlying the observed changes in gene expression.

Testosterone-induced genes were first associated with cellular changes and later with neural system changes.

We performed Gene Ontology (GO) term enrichment analysis to predict potential biological processes of the HVC affected by testosterone implantation at different time points (Fig. 3B and Supplementary File 8). After one hour of testosterone treatment, genes associated with processes such as circulatory system development (GO:0072359), cell development (GO:0048468), and neuron development (GO:0048666) were enriched, and genes associated with neurogenesis (GO:0022008) were enriched after three hours. Many processes associated with cellular anatomical changes showed continuous enrichment from T1h to T14d. Similar findings were observed in the KEGG pathway enrichment analysis (Figure 3 - Figure supplement 2A). We refined the above enrichment analyses with the foci on HVC cell types, neuronal protrusions, and neuronal activities. In cell type analysis, we observed enrichment for genes associated with "oligodendrocytes" among T3h upregulated genes (Fig. 3C, Supplementary File 9 and Supplementary File 10). In contrast, genes associated with "projection neurons" were enriched in the downregulated genes at both T3h and T8h. Although genes associated with "interneurons" and "microglia" were not enriched in the testosterone-regulated genes, the transcriptional changes in genes involved in GABA signaling (as described below) suggest that interneurons may have been affected. For testosterone-sensitive genes related to neuronal morphology, we found that genes associated with "myelin," and "spine" were enriched as early as one hour after testosterone treatment and almost at all later time points examined. We further investigated whether testosterone regulates chemical synapses and gap junctions and thus influences

inter-cellular communication by evaluating additional search terms, including gap junction, eight different neurotransmitters, their receptors, and genes involved in the biosynthesis of those neurotransmitters (Fig. 3). We found no enrichment of "gap junction" in the time window of our experiment. Among the eight neurotransmitters examined, only the genes associated with "glutamate" and "GABA" showed enrichment. Genes downregulated by testosterone were enriched for glutamate at T3h and T8h (Supplementary File 10). The genes associated with the inhibitory neurotransmitter GABA were enriched in the downregulated genes at T14d (Supplementary File 10).

At T14d, the biological processes of differentially expressed genes shifted dramatically. Alongside earlier active processes like neuronal development and cellular differentiation, broader functions such as organ formation and system development, including embryo morphogenesis (GO:0048598) and animal organ development (GO:0048513), emerged. Additional GO term enrichment analysis focusing on 4,050 genes only differentially regulated at T14d also revealed mainly system-level processes (Figure 3 - Figure supplement 2B). These observations suggest potential significant changes throughout the entire HVC after around 14 days of testosterone treatment. The only process at the system/organ level that was triggered early, immediately after the start of testosterone treatment, and continued throughout HVC development was the development of the circulatory system (GO:0072359). This emphasizes the importance of the blood system both for the differentiation of cells/neurons and the differentiation of the entire HVC system. Among genes associated with ion transport (GO:0006811), which was enriched only at T14d, genes encoded potassium ion channels, especially those responsible for inward rectifying (such as *KCNAB1*, *KCNJ3*, *KCNJ5*, *KCNJ8*, *KCNK10*, *KCNK16*, and *KCNK17*) were only upregulated at this time point. Such genes are highly differentially expressed in the HVC of male zebra finches (Lovell et al., 2013).

Identification of key genes and gene networks for testosterone-induced anatomical and behavioral changes.

We used WGCNA (weighted gene correlation network analysis) (Langfelder and Horvath, 2008, 2012), an unbiased clustering method, to identify functional units of gene co-expression networks relevant to testosterone-induced morphological and behavioral changes. We constructed an overall gene network composed of the HVC transcriptomes of testosterone-treated animals (Table 1). In the network, 12,360 genes were clustered into 14 modules by the WGCNA procedure (Fig. 4A and Figure 4 – Figure supplement 1). After module identification, WGCNA integrates gene expression data with morphological (HVC volume) and behavioral (song parameters) data to find modules that correlate strongly with the given parameters.

The "turquoise" module (an arbitrary name given by the "WGCNA" R package) was significantly and positively correlated with duration of testosterone implantation, HVC volume, song rate, song length, and the number of syllables in a song (Fig. 4A and Supplementary File 11). Eight other modules were significantly correlated with at least two song-related parameters. For example, the member genes of the "yellow" module was negatively correlated with song length, the number of syllables per song, and syllable repetition rate.

The "turquoise" module was the biggest module with 6,480 member genes (Supplementary File 11) and had the greatest average intramodular connectivity among the 14 modules, meaning members of this module are more likely to co-express than members of other modules (Figure 4 – Figure supplement 1). GO-term enrichment analysis showed it was highly associated with anatomical structure morphogenesis (GO:0009653, Bonferroni-adjusted P-value = 8.2×10^{-17}). Many genes of the "turquoise" module have been associated with testosterone-induced angiogenesis and neuron recruitment of HVC (Hartog et al., 2009; Kim et al., 2008; Louissaint et al., 2002; Rasika et al., 1999; Rasika et al., 1994), including brain-derived neurotrophic factor (*BDNF*), vascular endothelial growth factor (*VEGFA* and *VEGFC*) and VEGF receptors (*KDR*, *FLT1*, *FLT4*), insulin-

like growth factor 1 (*IGF1*), and matrix metallopeptidases (*MMP2* and *MMP9*) (Fig. 4B and Fig. 3A). Chondroitin sulfate proteoglycan 4 (*CSPG4*), the main component of perineuronal nets, has been associated with the closure of the sensitive period of song development (Cornez et al., 2020). In addition, 20 steroidogenesis enzymes were members of this module, such as hydroxysteroid dehydrogenase (*HSD3B2*), 17α-hydroxylase (*CYP17A1*), 17β-hydroxysteroid dehydrogenase (*HSD17B12*), aromatase (*CYP19A1*) and 5α reductases 2 (*SRD5A2*), as well as steroid receptors such as estrogen receptors (*ESR1* and *ESR2*), androgen receptor (*AR*), and G protein-coupled receptor family C group 6 member A (*GPRC6A*), which might mediate the non-genomic effects of androgens (Pi et al., 2010). Thus, the unbiased clustering method, which integrates the transcriptomes with behavioral and anatomical measurements under the influence of testosterone, was able to assign functionally relevant genes into a module, even though most of the genes were transiently regulated.

Transcription factor Sp8, a hub-gene.

Transcription factors are among the top 10 most connected genes in 10 of the 14 modules. In the turquoise module, approximately 10% of the most connected genes (intramodular connectivity higher than the 90th percentile) were transcription factors, and the most connected gene was *SP8*, a zinc-finger transcription factor of the SP/KLF family. It is required for the survival of pallial progenitor cells during corticogenesis (Limame et al., 2014; Zembrzycki et al., 2007), crucial in angiogenesis (Safe and Kim, 2008), CNS development (Bell et al., 2003; Gaborieau et al., 2018), as well as adult neurogenesis in mice (Waclaw et al., 2006). *SP8* was up-regulated after two weeks of testosterone treatment, a time point when the regulated genes were highly associated with anatomical changes at systemic levels (Fig. 3A and 3B).

To evaluate the potential direct regulation of SP8 on its highly connected genes in the "turquoise" module, we examined the presence of SP8 binding sites (V$SP1F) in the promoter sequences of 1,151 genes (adjacency > 0.5) using the “Genomatix-overrepresented TFBS tool”. SP8

binding sites are enriched in the input sequences and potentially exist in the promoter sequences of 625 genes, including *VEGFA* and *ESR2* (Supplementary File 12). Considering transcription factors can regulate gene expression in a combinatorically (Reményi et al., 2004), we identified potential interacting partners among these genes using the Search Tool for the Retrieval of Interacting Genes/Proteins (STRING) database. The database identified 11 proteins that might physically interact with SP8 based on bioinformatics evidence (Fig. 4C), including two transcription cofactors EED and SIN3A, and four transcription factors with three belonging to the GATA family (*GATA2*, *GATA3*, and *GATA4*). We then evaluated the likelihood of SP8 forming a transcription factor complex with GATA using the "Genomatix-overrepresented TFBS tool" module search function. Binding sites for complex V$GATA-V$SP1F were enriched in the promoter sequences of the 1,151 genes and potentially present in 169 submitted genes, including *VEGFA* and *ESR2* (Supplementary File 13).

The SP family plays an important role in estradiol-dependent gene regulation in breast cancer cell lines (Safe and Kim, 2008) and the presence of estrogen receptors enhanced the binding of the SP family (Fuentes and Silveyra, 2019). Therefore, we analyzed the promoter sequence of SP8, extracted from the canary genome, to investigate potential direct modulation by nuclear steroid receptors. The MatInspector tool of the Genomatix software suite identified two potential EREs (V$ESR2.01) in the *SP8* promoter, suggesting potential direct modulation by ESR2 in canaries. No ARE was found in the *SP8* promoter. Since both *ESR2* mRNA (1.80 fold) and *SP8* mRNA (1.75 fold) were significantly only upregulated at 14 d (Fig. 3 – Figure supplement 1), we localized *SP8* and *ESR2* mRNAs in specific neuronal populations within HVC of T14d birds, using high-sensitivity triple fluorescent *in situ* hybridizations (RNAScope®, see Methods) targeting both *SP8* and *ESR2* transcripts, as well as *VGLUT2* (also known as *SLC17A6*, Fig. 5) and *GAD*2 mRNAs (Figure 5 – Figure supplement 1). We observed a sparse expression of *ESR2* transcripts in HVC. These were expressed in populations of both *VGLUT2* mRNA-positive and *VGLUT2* mRNA-negative cells (Fig.

5). *SP8* mRNA was detected in a population of cells, mainly formed by *VGLUT2* mRNA-negative cells (Fig. 5A, 5B1, 5B2) which also expressed GAD2 mRNAs (Figure 5 – Figure supplement 1), and a lower fraction of *VGLUT2* mRNA-positive cells, which expressed lower numbers of *SP8* transcripts (Fig. 5B3). Overall, both *SP8* and *ESR2* mRNAs exhibited low expression levels in HVC, and co-localized in a subset of cells, predominantly GABAergic cells (Fig. 5B and Figure 5 – Figure supplement 1). *ESR2* has not previously been found in the HVC of songbirds (Bernard et al., 1999), possibly due to its transient expression after testosterone treatment. The co-expression of *SP8* and *ESR2* in HVC cells warrants further investigation to better understand their relationship and potential interactions in the context of testosterone-induced changes. At later stages of song development, steroid-controlled hub genes such as SP8 might enhance testosterone-induced gene cascades, in addition to direct parallel control of genes by androgen and estrogen receptors.

Discussion

We investigated the progression of transcriptomic changes in the song control nucleus HVC at various time points during testosterone-induced song development in female canaries, alongside changes in HVC volume and song. Our results reveal that the HVC exhibited extensive gene expression changes (2,652 genes) within one hour of testosterone exposure, preceding any noticeable changes in song development. These differentially expressed genes, from T1h to T3d, were primarily related to neuronal and cellular differentiation, including angiogenesis. As song development progressed, gene regulation associated with neuronal and cellular processes persisted. The scope of testosterone-related gene regulation broadened slightly to nervous system development at T7d (2,472 differentially expressed genes) and expanded substantially to organ/system (HVC) development at T14d (7,702 differentially expressed genes). Interestingly, the most extensive transcriptional changes occurred at T14d when the song pattern and HVC phenotype closely resembled those of singing male canaries.

Only 1.6% (153 genes) of the total 9,710 differentially expressed genes were consistently differentially regulated by testosterone across all time points, while over 50% of the genes were differentially regulated only at one time point. These findings suggest that distinct developmental stages of HVC and song differentiation require time-specific gene networks. The substantial number of genes that could be directly modulated by androgen and estrogen receptors, the presence of these receptors in about 60-70% of all HVC neurons (see below), and their increased expression at T14d all point to massive, parallel regulation of numerous genes, including other transcription factors, in the HVC by androgen and estrogen receptors.

Rapid, transient, and long-term constant regulation of extensive transcriptomes after testosterone treatment.

The HVC, a brain region with 30,000 to 50,000 cells inclusive of neurons, glia, and endothelial cells, expresses over 10,000 genes, representing approximately two-thirds of the known protein-coding genes in the canary genome (Frankl-Vilches et al., 2015). About 55% of cells in the canary HVC express androgen receptors, and around 25% express estrogen receptors (Gahr, 1990a, b; Johnson and Bottjer, 1993, 1995). Some express both receptor types (Gahr, 1990b), suggesting that about 60-70% of the HVC cells express androgen and/or estrogen receptors, making them direct targets for testosterone and its metabolites. Local conversion of testosterone to 5α-DHT and 17β-estradiol is possible due to the expression of 5α-reductase and aromatase in HVC (this study; (Metzdorf et al., 1999)). While we expected these metabolites to influence multiple gene networks, the degree of extensive transcriptional regulation and its rapid onset were surprising. Testosterone reaches the HVC in about 30 minutes after implantation, based on previous autoradiographic studies (Arnold et al., 1976; Marynick et al., 1976). Thus, it is even more surprising that testosterone altered the expression of more than 2,700 genes in an hour or less. The number of differentially expressed genes remained at this level until about 14 days after treatment when it roughly tripled to 7,702 (Fig. 3A).

Interestingly, down-regulated genes increased by 23.5% between 7 and 14 days, while up-regulated genes increased by 604.9%.

The extensive and rapid gene expression regulation across various functions presents a challenge to the traditional model of androgen and estrogen receptor-mediated gene regulation, where a few hub genes modulate the majority of others. It's important here to note some limitations of our promoter sequence analyses. The overrepresentation analysis, which compared the prevalence of androgen and estrogen binding sites in the promoter sequences of T1h testosterone-sensitive genes to a random sample from the canary genomic background, suggests the potential for rapid, parallel gene regulation by these receptors. However, these analyses may not fully represent the complexity of this process, considering that binding sites occupied by androgen and estrogen receptors can be up to 10 kb from transcription start sites, beyond the genomic range examined here (Bourdeau et al., 2004; Farcas et al., 2020; Stelloo et al., 2019; Takayama et al., 2007; Wilson et al., 2016). Further, the complexity of transcription factor binding influenced by variables such as chromatin accessibility, cofactors, and epigenetic modifications, introduces additional layers of regulatory control that our methods may not fully capture. Therefore, these findings should be validated experimentally using techniques such as ChIP-seq or CUT&RUN.

Within an hour, androgen and estrogen receptors regulate transcription factors that may amplify testosterone-induced effects (**Fig. 2**A). This indirect gene expression control could be particularly pronounced after 14 days of testosterone treatment, when the expression of a large number (730) of transcription factors changes. Single-cell transcriptomes would help determine how testosterone regulates gene expression in cell types expressing or lacking androgen and/or estrogen receptors.

The majority (52.3%) of the testosterone-sensitive HVC genes (4,798 of 9,710) were regulated only at a single time point after testosterone administration, suggesting that specific gene

networks are regulated by androgen and/or estrogen receptors at different time points or are induced by previously regulated networks that no longer require testosterone. Although we didn't explicitly investigate this, the fact that song development halts when testosterone implants are removed (Vellema et al., 2019), implies the continuous presence of testosterone or its metabolites is necessary for gene regulation throughout song development.

Androgen- and estrogen-receptor binding to DNA is highly tissue- and context-specific (Pihlajamaa et al., 2015; Pihlajamaa et al., 2014), implying potential time-dependent and tissue-specific regulation during HVC differentiation. Over 61% of the top ten GO terms across the six time points examined are active as early as one hour after testosterone administration (**Fig. 3**C), suggesting a transient impact on most genes involved in these functions, despite some functions being regulated more long-term by testosterone (**Fig. 3**B and Figure 2 - Figure supplement 1). The dynamic and transient nature of HVC transcriptomes during song development might reflect the observation that different anatomical features of HVC neurons, glial cells, and vessels change in parallel with song features at different time points ((Hartog et al., 2009; Louissaint et al., 2002; Nottebohm, 1980; Rasika et al., 1994; Vellema et al., 2019) and this study, see below).

The extensive effects of testosterone on HVC gene expression surpassed our expectations, as we did not expect such a large number of differentially expressed genes. A comparison of our results with other studies on the effects of testosterone treatment or seasonal phenotypes on the transcriptomes of both peripheral tissues and the central nervous system in other animals, including birds, amphibians, fish, and rodents, revealed that typically far fewer differentially expressed genes are reported, with most studies reporting fewer than 2000 genes (Bao et al., 2019; Bissegger et al., 2014; Carrier et al., 2015; Cheviron and Swanson, 2017; Dopico et al., 2015; Faber-Hammond et al., 2015; Félix et al., 2020; Morey et al., 2016; Peterson et al., 2013; Quintela et al., 2015; Sharma et al., 2019; Zhang et al., 2016; Zhao et al., 2021). A comparably large effect was only reported for seasonal changes in the testes (Tian et al., 2019). The discrepancy in the number of genes influenced

by testosterone in different species and tissues may be due to several potential reasons, including species-specificity, cellular diversity, and technical variations. However, in the context of the HVC, our results in terms of the number of differentially expressed genes are the most striking and extensive reported in the CNS literature. This may be due to the HVC's cellular diversity compared to peripheral tissues (Colquitt et al., 2021) or the extensive expression of androgen and/or estrogen receptors in about 60 to 70% of HVC neurons (Gahr, 1990a, b; Johnson and Bottjer, 1993, 1995), which should include most HVC neuron types.

The substantial number of testosterone-induced differentially expressed genes observed, particularly at later stages (T14d) of song development in the adult female canary HVC, mirrors patterns seen in embryonic organ formation. This parallel, underscored by its prominence in our Gene Ontology (GO) analysis (Fig. 3), implies that testosterone (or estrogen) might trigger adult behaviors, like parenting and courtship, through more extensive transcriptomic restructuring and functional modifications in relevant brain areas than previously considered.

The testosterone-driven changes in female HVC morphology and function represent some of the most notable modifications known in the vertebrate brain. However, how this extensive, testosterone-induced gene regulation in the HVC applies to other seasonally testosterone-sensitive brain areas remains to be seen. Endpoint analysis of testosterone-induced singing in male canaries during the non-reproductive season also indicates considerable regulation of HVC transcriptomes (Frankl-Vilches et al., 2015; Ko et al., 2021). It's important to note that the HVC, despite its central role, is just one part of the song control system. Singing requires the coordinated functionality of at least three brain areas within the descending song motor system (Wild, 2004). Given that these areas, along with the sound-producing organ, also express androgen receptors (Gahr and Wild, 1997; Godsave et al., 2002), testosterone's influence extends to regulating a substantial portion of the canary gene pool to facilitate singing.

Testosterone-driven transcriptomic changes, neural changes, and song differentiation. Singing in canaries initiated around four days after testosterone treatment, with the song progressively evolving from early sub-songs to plastic songs, characterized by increasing stereotypy of syllables, syllable repetition rate, and total number of syllables in a song (Fig. 1 and Figure 1 – Figure supplement 1). Despite individual variability, by the end of our 14-day experiment, the plastic songs produced— already featuring long sequences, high repetition rates, and multiple syllables with short pauses—closely resembled typical canary songs post-testosterone treatment. The transcriptional changes in the HVC strongly correlate with testosterone treatment and song development. Specifically, changes on days 1 and 3 likely prime the HVC for early sub-song production, while those on day 7 appear to facilitate late sub-song singing and HVC circuit differentiation essential for plastic song production. Furthermore, changes on day 14 could be associated with the production of plastic songs and the differentiation processes contributing to fully stereotyped songs emerging from 14 days onwards (Vellema et al., 2019).

Interestingly, testosterone treatment initiated a cascade of gene regulation in functional processes crucial to song development. Some of these processes were activated immediately following administration, while others displayed a delayed onset. While the rapid transcriptional changes at T1h could potentially trigger homeostatic responses to temper testosterone activity, they also activated many genes implicated in cellular plasticity. These genes are involved in cytoskeletal organization and cellular morphogenesis, as highlighted by our Gene Ontology (GO) analysis (Fig. 3C). Such findings resonate with previous research, underscoring the influence of testosterone on angiogenesis, neurogenesis, and gliogenesis (Goldman and Nottebohm, 1983; Louissaint et al., 2002), in addition to its impact on permanent neuron populations in the HVC (Gahr, 1990b). Rapid neuronal differentiation was evidenced by the enrichment of differentially expressed genes related to "dendrites," "axon," and "spine" just three hours post-treatment, suggesting that testosterone plays a critical role in this process (Fig. 3C, 3D). Balanced activity of excitatory and inhibitory neurons in

the HVC might be important for HVC networks in song control. We observed enrichment of genes associated with "glutamate" (downregulated) at early time points (T3h and T8h) (Fig. 3D). At the earliest stage, the only system-level process initiated was vascular system development. The vascular endothelial growth factor (*VEGF*) receptors, *KDR* and *FLT4*, had higher expression in T1h animals than in controls (Fig. 2E). Additionally, *FLT1* (another VEGF receptor) was upregulated at T8h, while *VEGFA* and *VEGFC* at T3d.

At the system level, GO term analysis showed that differentially expressed genes related to circulatory system development (GO:0072359) were enriched at all time points starting at T1h while system (organ) development (GO:0048731, GO:0048513) concerning the entire HVC was massively regulated at 14 days of treatment (Fig. 3C). Our results align with the previous finding that testosterone triggers HVC vasculature development (Hartog et al., 2009; Louissaint et al., 2002), suggesting processes such as expanded vasculature are important for neuronal differentiation and increased neuronal activity. These cellular differentiation processes, which begin within the first days of testosterone treatment, may contribute to the onset of song pattern generation, and precede the extensive systemic changes in the HVC of female canaries treated with testosterone over an extended period (T14d).

As canaries progressed from subsong to plastic song around T7d, a period characterized by increased song stereotypy and the emergence of typical HVC functions such as syllable sequencing, we observed enrichment in the transcription of genes tied to circulatory system development (GO:0072359, Fig. 3B). This stage coincides with the secretion of VEGF by HVC endothelial cells, driven by the testosterone metabolite 17β-estradiol (but not 5α-DHT), which then stimulates the VEGF signaling pathway, angiogenesis, and BDNF release (Louissaint et al., 2002). BDNF, which was upregulated in the T7d transcriptome, regulates the recruitment and survival of adult-born neurons (Rasika et al., 1999). Concurrently, genes related to neuronal differentiation maintained differential expression at T7d. In light of these changes, it's likely that the HVC undergoes ongoing,

subtle morphological modifications after an increase in testosterone levels, contributing to the HVC phenotype. Notably, the volume change observed in T7d animals wasn't statistically significant from control animals; only three T7d birds exhibited an increased HVC volume akin to T14d animals (Fig. 1F). Further exploration is warranted to ascertain the specific electrophysiological properties altered in HVC neurons during this stage of song development.

By T14d, marked neuroanatomical changes, such as visible enlargement of the HVC(Fig. 1F) (Gahr, 1990a; Gahr and Metzdorf, 1997), were evident, aligning with previously documented data on testosterone-implanted female canaries implanted with testosterone for three weeks or longer (Fusani et al., 2003; Hartog et al., 2009; Madison et al., 2015; Nottebohm, 1980; Rasika et al., 1994). This morphological transformation was accompanied by a threefold increase in differentially expressed genes, highlighting substantial transcriptional modifications in the HVC. The precise neuroanatomical adaptations contributing to these HVC changes remain unidentified, but possible factors include synaptic pruning, as indicated by the persistent downregulation of "spine"-related genes (Fig. 3C). Recent research has revealed a decrease in HVC dendritic spine density following testosterone administration, implying that synaptic pruning in the HVC contributes to the crystallization of female canary song (Vellema et al., 2019). Additionally, the upregulation of ion channel genes, such as inward rectifying potassium channels, at 14 days of treatment might stabilize the electrical properties of HVC neurons. This stabilization could minimize variability in neuronal networks, potentially leading to the observed increase in song pattern stability at this stage.

The cellular and system-level differentiation of the HVC on day 14 (T14d) correlates with the significant increase in song length and syllable rate between days 7 and 14. This change is characterized by longer, uninterrupted sequences of syllables and a higher syllable rate, both indicative of the HVC's critical role in the sequential temporal organization of syllables (Basista et al., 2014; Goldin et al., 2013; Hahnloser et al., 2002). Simultaneously, the striking expansion of differentially expressed genes in the HVC may be further amplified by the heightened singing

activity of T14d females. Indeed, singing activity itself can boost the expression of the immediate early gene ZENK in the canary HVC (Jarvis and Nottebohm, 1997), and potentially other transcription factors, thereby possibly regulating further gene cascades (Choe et al., 2021; Whitney et al., 2014). However, our experimental design, which induced singing via testosterone administration, was unable to differentiate between the effects of testosterone on HVC and those elicited by testosterone-dependent song production. The significant increase in singing activity, which was observed only after day 9, suggests that the expanded transcriptomes at 14 days might be particularly influenced by singing. There were 4050 genes exclusively regulated at T14d, primarily associated with system-level processes. Thus, we assume that these genes are not primarily induced by increased song activity, as one would expect for genes related to metabolic functions and cellular homeostasis. Unexpectedly, the system-level organization of the HVC at this later stage of testosterone-induced song development does not appear to be due to the accumulation of many cell-level (neuronal) mechanisms but instead involves a new group of temporally regulated genes. The intricate interactions between testosterone, song production, and their combined influence on the HVC underscore a compelling direction for future research, enhancing our understanding of neuroanatomical and transcriptional changes associated with singing behavior.

Conclusions.

Testosterone treatment rapidly triggered extensive transcriptional changes in the HVC of female canaries and dramatically altering song. Following the swift onset (1 hour or less) of the transcriptional changes, the transcriptomes underwent significant transformations several times during the two-week song development. This progression of transcriptomes shows that most genes were regulated only at specific stages of HVC and song development. The differentially expressed genes are associated with numerous biological functions, with systemic functions emerging primarily after prolonged testosterone treatment. This suggests that adult song development may involve a

restructuring of the entire HVC, potentially affecting a variety of HVC cell types, rather than only changing some neuronal populations or cellular components. These changes may be influenced by parallel direct regulation of thousands of genes by androgen and estrogen receptors, as well as by other hub genes such as *SP8* that are themselves under steroidogenic control. Our study identified extensive gene networks that strongly correlate with behavioral and neuroanatomical changes during the song development of adult birds.

Materials and Methods

Animals.

Forty-two adult female canaries (*Serinus canaria*) were used in this study (see Table 1). Adult female canaries (*Serinus canaria*, at least one-year-old) were bred in the animal facility of the Max Planck Institute for Biological Intelligence, Seewiesen, Germany. Housing and welfare of the animals followed the European Directives for the protection of animals used for scientific purposes (2010/63/EU), and protocols were approved by the Government of Upper Bavaria under AZ-No. 55.2/54-2531-68/12. The ARRIVE guidelines (Kilkenny et al., 2010) were followed and a checklist was provided with the manuscript.

The sex of the animals was confirmed by PCR using primers P2 and P8 for the CHD genes (Griffiths et al., 1998) and by visual inspection of the female reproductive system after killing. Food and water were always provided *ad libitum*. Birds were kept under local light conditions. Six to eight weeks before the experiment started (beginning in September at the earliest), the light schedule was gradually changed to short-day conditions (light: dark = 9:15 hours). After the birds became accustomed to the short-day light cycle, singing was monitored. Birds were divided into a control group and six experimental groups; the numbers of birds per group are summarized in Table 1.

Testosterone was implanted into the experimental groups for different periods (T1h, T3h, T8h, T3d, T7d, T14d, see Method: Testosterone Implantation).

Song monitoring.

About 5% of female canaries sing spontaneously without hormone manipulation (Ko et al., 2020). To ensure that vocal activity in our experiment was indeed triggered by testosterone implantation, birds used in this study were housed alone in sound-attenuated boxes (70 × 50 × 50 cm) and all vocalizations were recorded continuously for two weeks before testosterone implantation and until killing. The microphone (TC20, Earthworks, Milford, New Hampshire) in each silenced box was connected to a PR8E amplifier (SM Pro Audio, Melbourne, Australia) that fed into an Edirol USB audio recording device (Edirol UA 1000, Roland, Los Angeles, California) connected to a computer. Vocalizations were recorded at a sampling rate of 44.1 kHz and a resolution of 16 bits using Sound Analysis Pro 2011 software (Tchernichovski et al., 2000).

Song analysis.

Birds treated with testosterone began singing unstable so-called subsongs on average on day 4. Therefore, song data refer to animals in the T7d and T14d groups. Nine hours of recordings were analyzed per day. We analyzed all recordings from day 0 until the birds were killed (until the seventh or fourteenth day). For the analysis of songs and song activity for the first 7 days, we combined data from T7d and T14d birds because their songs did not differ significantly (Figure 1 – Figure supplement 3, Supplementary File 2, and Supplementary File 3). Song analysis was performed using Multi_Channel_Analyser (MCA), a custom program with a graphical user interface written in MATLAB (version R2016b, Mathworks), as described previously (Ko et al., 2020) and available to the public (https://doi.org/10.5281/zenodo.1489098). Briefly, MCA loads song files and generates sound spectrograms using the fast Fourier transform with a sliding time window of 294 samples and an overlap of 128 samples between adjacent sections. These settings result in a spectrogram with a

resolution of 150 Hz on the frequency axis and a resolution of 3.76 milliseconds on the time axis. Due to background noise, syllable recognition was performed in three steps. First, sound segments (songs and calls) were manually selected by visual inspection. Second, song segments were selected if the sound segment was longer than 2 seconds. Third, syllables within the selected segments were automatically detected using MCA by setting the following parameters in MCA: "High-pass filter" to 2.0 kHz, "Threshold_wave_amplitude" to 0.001, and "Threshold_syllable_freq" to 50 Hz. Sounds shorter than 5 milliseconds (ms) were removed.

Digital samples of the recognized syllables were exported and used to calculate sound features. As in the previous study (Ko et al., 2020), four song-level and four syllable-level parameters were considered. Song-level parameters included three temporal features: Song length, number of syllables in a song, syllable repetition rate, and a spectral feature, the slope coefficient (α) (Gardner, 1978; Gisiger, 2001; Voss and Clarke, 1975). Syllable-level parameters include two temporal features, syllable length and syllable spacing, and two spectral features, peak frequency, and Wiener entropy. Song length was calculated by subtracting the timestamp at the end of the last syllable and the timestamp at the beginning of the first syllable of a song. The syllable repetition rate was defined as the number of syllables in the song divided by the song length in seconds. Syllable length was calculated by subtracting the timestamp at the end of the syllable and the beginning of the syllable. The interval between syllables was calculated by subtracting the timestamp at the beginning of the following syllable and the end of the syllable. The peak frequency was the frequency at which the power in the spectrogram of a syllable was highest. Wiener entropy is a unitless measure of signal noise that provides a measure of the width and uniformity of the power spectrum. To obtain a broader range, we used the log-transformed Wiener entropy. In this case, a Wiener entropy of 0 represents white noise and the value infinity represents pure tone (Tchernichovski et al., 2000).

Testosterone implantation.

We custom-made the testosterone implants by packing testosterone (86500, Sigma-Aldrich, Saint

Louis, Missouri) into a 7-mm-long SilasticTM tube (Dow Corning, Midland, Michigan; 1.47 mm inner diameter, 1.96 mm outer diameter, 0.23 mm thickness). Both ends of the SilasticTM tube were sealed with silicone elastomer (3140, Dow Corning). After sealing, the implants were cleaned with 100% ethanol to remove any testosterone particles. To ensure that no leakage occurred, the implants were placed in ethanol in a fume hood overnight. Implants that were moist were discarded. One day before implantation, implants were incubated overnight in 0.1 M phosphate-buffered saline (PBS) to ensure the immediate release of testosterone upon implantation (Rasika et al., 1994). We started subcutaneous implantation immediately after turning on the light at 8:30 am, with an interval of 20 minutes between each bird, considering the time needed on the day of euthanasia. Control animals were implanted with empty 7-mm silicone tubes that were also sealed with silicone elastomer. After the designated implantation period (1h, 3h, 8h, 3d, 7d, or 14d, Table 1), the birds were killed with an overdose of isoflurane, body weight was recorded, and the brains and oviducts were dissected, weighed, frozen on dry ice, and stored at -80□ until further use. The oviducts of eleven birds were no collected or the weights were not measured during dissection. The testosterone implants were all present at the time of euthanasia and held testosterone.

Radioimmunoassay of plasma androgens.

To confirm that systemic hormone manipulation increases circulating androgen levels, we performed a radioimmunoassay on blood samples collected before and after testosterone implantation (Fig. 1A). During the experiment, blood samples (approximately 100 μl) were collected twice from the wing vein for testosterone analyses, once approximately 4 days before testosterone implantation, and once immediately before killing. All blood samples were collected between 8 and 11 am, and within 3 min to avoid handling effects (Wingfield et al., 1982). Blood samples were centrifuged (5,000 rpm, 10 min) to separate plasma from blood cells. Testosterone metabolites in plasma were measured by radioimmunoassay using a commercial antiserum to testosterone (T3-125, Endocrine Sciences, Tarzana, California), as described previously (Goymann et al., 2002). Standard curves and sample

concentrations were calculated with Immunofit 3.0 (Beckman Inc. Fullerton, California) using a four-parameter logistic curve fit and corrected for individual recoveries.

The testosterone concentrations were assayed in duplicates in four separate assays. The mean extraction efficiency for plasma testosterone was 84.0 ± 6.8% (mean ± SD, N = 120). The lower detection limits of the testosterone assays were 0.35, 0.34, 0.44, and 0.32 pg per tube, and all the samples were above the detection limit. The intra-assay coefficients of variation of a chicken plasma pool were 4.4%, 4.1%, 9.8%, and 2.6%. The inter-assay coefficient of variation as determined by the variation of the chicken plasma pool between all the assays was 4.3%. The testosterone antibody used shows significant cross-reactions with 5α-dihydrotestosterone (44%), our measurement might include a fraction of 5α-DHT and thus we referred to the measurement as plasma androgen level.

Testosterone implants increased plasma androgen levels in all testosterone-treated groups (Supplementary File 2 and Supplementary File 3). In contrast, pre-implantation levels were statistically similar in all groups (159 ± 449 pg/ml, mean ± standard deviation (SD)). Implantation increased plasma androgen levels by at least 28-fold above baseline (range: 17 to 88 ng/ml) after only one hour. Plasma androgen levels after implantation for all testosterone-treated groups were not statistically different from each other (plasma androgen levels after implantation for each group: CON 0.0472 ± 0.0240; T1h 46.9 ± 28.2; T3h 53.9 ± 14.8; T8h 35.6 ± 24.0; T3d 20.4 ± 4.47; T7d 14.8 ± 3.29; T14d 9.31 ± 2.94 ng/ml).

Brain sectioning.

Brains were sagittal sectioned using a cryostat (Jung CM3000, Leica, Wetzlar, Germany) in either 40 μm × 4 + 20 μm × 2 (N = 17) or 50 μm × 4 + 14 μm × 3 (N = 33) sections. The thick sections (40 or 50 μm) were mounted on glass slides for subsequent microdissection of the tissue for microarray analysis, whereas the thin sections (20 or 14 μm) were mounted on RNase-free Thermo Scientific™ SuperFrost Plus™ slides (J1800AMNZ, Thermo Fisher Scientific, Waltham, Massachusetts) for

Nissl staining or RNAscope® in situ hybridization assay (Wang et al., 2012). All sections were stored at -80 °C until further processing.

Measurement of the HVC volume.

A set of thin serial sections (20 or 14 μm) were Nissl-stained (0.1% thionine solution) and covered with Roti-Histokitt II embedding medium (Roth). HVC areas were measured using ImageJ2 (Rueden et al., 2017) (Fiji distribution (Schindelin et al., 2012)). All brains were coded so that the evaluators had no information about the identity of individual brains and sections. Volumes were derived from summed-area measurements multiplied by section thickness and section spacing. The Nissl-stained sections of one T3d bird were in bad quality thus we did not quality the HVC volume of this bird.

RNAScope® *in situ* hybridization assay.

For RNAScope® *in situ* hybridization, three birds were used for a given probe at a given time point (3 slices for each bird). *In situ* hybridization for mRNA expression of *ALDH1A2*, *AR*, *HSD17B12*, *SRD5A2*, and *UTS2B* was performed on sections (20 or 14 μm thick) using the RNAScope ®2.0 HD Detection Kit (Advanced Cell Diagnostics, Newark, California) (Wang et al., 2012) according to the protocols indicated by the manufacturer. Stained tissue sections were imaged using a Leica DM6000 B microscope (Leica). Quantification was performed using ImageJ2 (Fiji Distribution (Rueden et al., 2017; Schindelin et al., 2012)). We measured the area of accumulated chromogenic particles in the stained HVC sections for all probes and normalized the values using the area of the HVC region of the same section. We used the Color Threshold function (color space: RGB; red channel: 0 to 47; green channel: 0 to 165; blue channel: 0 to 160) to select the accumulated chromogenic particles and the Analyze Particles function (minimum size = 8 μm^2) to count the number of accumulated chromogenic particles and the area occupied by the chromogenic particles (user-defined macro file: "Marco_quantify_density_singleProbes_quantify_area.ijm").Our macro files are available on GitHub (https://github.com/maggieMCKO/TimeLapseTestoFemaleCanary/blob/ce9261d1cf96e7603517336

57434e499dea35174/RNAscopeQuantification/Marco_quantify_density_singleProbes_quantify_area.ijm).

RNAScope® fluorescent multiplex V2 assay (Advanced Cell Diagnostics) was used to visualize mRNA expression of *SP8*, *ESR2*, *VGLUT2* (*SLC17A6) and GAD2* following the protocols provided by the manufacturer. Probes were conjugated to Opal 520, Opal 570, Opal 650 fluorophores. Sections were counterstained with DAPI. The information of probes used was summarized in Supplementary File 14. The stained tissue sections were imaged using a Stellaris 5 confocal microscope (Leica) equipped with a white light laser and a 405nm laser and a HC PL APO CS2 40x/1.10 water immersion objective. Laser excitation wavelengths and emission filters were chosen to minimize cross-talks between channels. DAPI was visualized with an excitation wavelength of 405 nm and emission filter 430-547 nm. Opal dyes 520, 570, and 650 were visualized with excitation wavelengths of 491 nm, 550 nm and 627 nm and emission filters 496-550 nm, 552-621 nm, and 632-719 nm respectively. Images were acquired with a pixel size of 0.142 µm. *VGLUT2* staining allowed assessment of co-localization in *VGLUT2*-positive cells (glutamatergic). VGLUT2-negative cells mainly corresponds to putative GABAergic neurons, which express GAD2mRNA (Alcami et al., 2021). Since RNAScope V2 assay allows only triple-stainings, the GABAergic or glutamatergic identity of *SP8* and *ESR2* expression was analyzed in separate assays. Images were analyzed with ImageJ software.

Microarray procedures and annotation.

Forty-two adult female canaries (six birds per group) were planned for microarray analysis following the method proposed by (Pan et al., 2002). However, two of these birds were excluded because the RNA amount was not sufficient for the microarray hybridization, and one sample did not pass the filtering step during the WGCNA analysis (see below). Thus, thirty-nine female canaries were used for microarray analysis (see Table 1). The procedure was described in (Ko et al., 2021).

Briefly, we extracted total RNA by dissecting the HVC from the previously mentioned thick sections (40 or 50 μm) under a stereomicroscope, using adjacent Nissl-stained sections from the same bird as a reference. In a sagittal section, the HVC is situated ventral to the hippocampus and lateral ventricle, and caudo-dorsal to the lamina mesopallialis. We typically dissected about 20 slices per HVC and transferred the tissue into an Eppendorf tube containing 340 μl of RLT buffer mixture (with DTT, Qiagen, Valencia, California). We used these rather thin sections for dissection of HVC to avoid contamination of the samples with non-HVC tissues. RNA was then extracted using the RNeasy® Micro Kit (Qiagen) with the optional DNase digest step. The RNA quality was assessed using the Agilent Model 2100 Bioanalyzer (Agilent Technologies, Santa Clara, California) and the RNA concentrations were assessed using a Nanodrop 1000 spectrometer (Thermo Fisher Scientific). The RNA quality of all samples was of good quality (RNA integrity numbers (RIN) > 7). The purified total RNA samples (at least 100 ng per sample) were subsequently processed and hybridized using the Ambion WT Expression Kit (Thermo Fisher Scientific) and the Affymetrix WT Terminal Labeling and Controls Kit (Thermo Fisher Scientific). The resulting cDNA was hybridized to the Custom Affymetrix Gene Chip® MPIO-ZF1s520811 Exon Array, which has been used and validated in successfully cross-species (zebra finches and canaries) hybridization studies (Dittrich et al., 2014; Frankl-Vilches et al., 2015). Hybridization was performed for 16 hours at 45°C and 60 rpm in the GeneChip Hybridization Oven 640. The arrays were washed, stained, and scanned using the Affymetrix GeneChip Fluidics Station 450 and Affymetrix GeneChip scanner 3000 7G. The CEL files were generated using Affymetrix GeneChip Command Console® Software (AGCC), and for quality control, the success of individual hybridizations was assessed using the Affymetrix Expression Console™ software. The 5.7 million male zebra finch-specific probes spotted on our custom array correspond to approximately 4,711,133 probe sets and hence to 25,816 transcripts published in public databases (NCBI and Ensembl) (Warren et al., 2010). We annotated more than 90% of the transcripts to 12,729 human orthologous genes using publicly available databases

(Ensembl, GenBank, UniProt, and DAVID (Benson et al., 2005; Consortium, 2015; Flicek et al., 2014; Huang et al., 2008, 2009; Yates et al., 2016)), as well as commercial databases (v 21 El Dorado, Genomatix, Precigen Bioinformatics Germany GmbH (PBG), Munich, Germany). The microarray data generated in this study have been deposited in NCBI's Gene Expression Omnibus (Edgar et al., 2002) and are accessible through the GEO Series accession number GSE118522.

Analysis of differentially expressed genes.

ChipInspector software (v21, El Dorado Database vE28R1306, (Genomatix), Precigen Bioinformatics Germany GmbH (PBG)) was used to calculate differential expression between each experimental group and the control group. ChipInspector is a single probe-based analysis tool for microarray data that increase sensitivity compared to conventional probe-set-based analyses, such as robust multi-array analysis (Cohen et al., 2008; Tusher et al., 2001). We used the following parameters in ChipInspector: group-wise exhaustive comparison: Delta threshold (controlling false positive rate) was set at 0; the minimum coverage for each transcript was set at 10 significant probes; the minimum differential expression was $|\log_2(\text{fold change})| \geq 0.5$. The significantly differentially expressed transcripts obtained were annotated to human orthologous genes as described above. For transcripts belonging to the same genes, the average expression was calculated if all transcripts were regulated in the same way (e.g., all up-regulated or all down-regulated). If a gene contains both up- or down-regulated transcripts, transcripts of the minority direction were discarded (<40% of the total transcripts), and the average expression was instead calculated from the remaining transcripts (60% or more). Transcripts without human orthologous gene annotation were removed before subsequent analyses.

Considering our moderate sample sizes, we conducted a power analysis for each probe-set in the pairwise differential expression analysis. We first calculated the effect size using RMA-normalized expression from the CEL files (see the WGCNA section below), by computing group means and pooled standard deviations. We then employed the "pwr.t.test" function (two-sided, α set

to 0.05) from the "pwr" R package (v1.3-0) to estimate power for each probe-set. For each differentially expressed gene at each time point, we considered it a high power differentially expressed gene if at least one probe-set had a power ≥ 0.8. In total, 93% of differentially expressed genes identified by ChipInspector with |log2(fold change)| ≥ 0.5 had a power ≥ 0.8.

The differential analysis results agree with the published data at the overlapping time point (T14d, Fig. 2E): after two weeks of testosterone implantation, elevated mRNA levels of a vascular endothelial growth factor receptor (*KDR*) and brain-derived neurotrophic factor (*BDNF*) were reported (Louissaint et al., 2002). For further verification of the microarray results, we conducted RNAScope® *in situ* hybridization assay for several genes involved in testosterone metabolism, including androgen receptor (*AR*), 17β-hydroxysteroid dehydrogenase (*HSD17B12*), 5α reductases 2 (*SRD5A2*), and aldehyde dehydrogenase 1 family member A2 (*ALDH1A2*) (Wang et al., 2012). The quantifications were congruent with the microarray results (Fig. 2).

Analysis of overrepresented transcription factor binding sites.

Our analysis specifically targeted the overrepresentation of androgen and estrogen response elements (AREs and EREs). For this purpose, we extracted the promoter sequences of the testosterone up-regulated genes and the promoter sequences of the direct neighbors of SP8 identified by WGCNA (adjacency > 0.5). The promoter sequences were defined as 1,000 bp of genomic sequence upstream of the putative transcription start site, extracted from the canary genome (Frankl-Vilches et al., 2015; GenBank assembly accession: GCA_000534875; BioProject:PRJEB1766).

We utilized the "Toolbox for Overrepresented Transcription Factor Binding Sites" of the Genomatix software suite from Precigen Bioinformatics Germany GmbH (Cartharius et al., 2005; Genomatix; Quandt et al., 1995; Sui et al., 2005). This tool enabled us to identify overrepresented TFBSs and determine whether individual TFBSs or pairs were overrepresented in the input sequences compared to a background of randomly selected canary promoters, the number of which matches the number of input promoters. For our analysis, we selected the vertebrate TFBS matrix

library, and the curated zebra finch promoter sequences available in Genomatix were set as background for statistical purposes. The Z-score was calculated as the overrepresentation of canary TFBSs in the up-regulated gene promoters against the selected background, and this value was compared to the Z-score in the same number of randomly selected canary promoters. We did not control for GC content when selecting the random canary promoters because the motifs of interest, ARE and ERE, are not predominantly GC-rich. Consequently, any overrepresentation of these motifs is unlikely to be due to an abundance of GC-rich promoters.

Additionally, we used the module search function of the TFBS-Genomatix toolbox to assess the likelihood that SP8 forms a transcription factor complex with GATA. This was done by searching for TF binding sites within 10 to 50 bp (center to center) of each other.

Identification of AREs and EREs using MatInspector tool.

We utilized the MatInspector tool from the Genomatix software suite (Cartharius et al., 2005) to identify potential AREs (matrix family: V$GREF/ARE.01, V$GREF/ARE.02, V$GREF/ARE.03, and V$GREF/ARE.04) and EREs (matrix family: V$EREF/ER.01, V$EREF/ER.02, V$EREF/ER.03, V$EREF/ER.04, V$EREF/ESR2.01) in the promoter sequences (1,000 bp upstream of the putative transcription start site) of 38 up-regulated transcription factors at T1h, which were available from the canary genome (see above), using default settings.(Cartharius et al., 2005)

Enrichment analysis of Gene Ontology (GO)-terms and KEGG pathways.

We used ClueGO v2.5.0, an application developed under the Cytoscape environment v3.5.1 (Bindea et al., 2009; Shannon et al., 2003), to predict the putative biological functions of genes of interest. This software performs hierarchical analyses of GO term enrichment and fuses GO terms of similar functions. Similarly, we performed KEGG pathway enrichment analysis. Enrichment was determined with a right-sided test and corrected with the Bonferroni step method considering multiple comparisons. Results were plotted using the R package ggplot2 (Wickham, 2009).

Enrichment analysis of genes related to cell types, neuronal processes, and neurotransmitters.

We searched 33 terms associated with cell types, neuronal protrusion types, and biosynthesis of neurotransmitters and neurotransmitter receptors and downloaded the gene lists associated with each search term (Supplementary File 9), using the "Genes and gene products" tool of the AmiGO 2 database (v2.4.26, release date 2017-07-05 (Ashburner et al., 2000; Consortium, 2017)). Subsequently, we used the Fisher's exact test ("Fisher-Test", alternative hypothesis set to "greater") to determine whether enrichment of a search term (genes associated with the term) is observed in the list of differentially expressed genes of a given time point. We used the total number of genes detected in our microarray (12,018 genes) as the universe in the Fisher's exact test. The P-values were adjusted for multiple comparisons by Bonferroni's method using the "p.adjust" function. We performed the calculations in R (Team, 2020) and visualized the results using the ggplot2 R package (Wickham, 2009).

Weighted gene co-expression network analysis (WGCNA).

WGCNA R package v1.51 (Langfelder and Horvath, 2008, 2012) was used to identify functional units of gene co-expression network that are relevant for the testosterone-induced morphological and behavioral changes (traits, Fig. 4A). WGCNA calculates the network adjacency matrix based on the correlation of gene expression data and assigns genes into modules (sub-networks within the overall network) based on the topological overlap matrix from a given network adjacency matrix. The adjacency value can be seen as a proximate indicator for connection strengths among the nodes (genes) in the network: a pair of highly correlated genes have an adjacency value of 1, indicating the pair is likely co-expressed at a given time. After module identification, WGCNA integrates the gene expression data with the morphological and behavioral data to identify modules strongly correlated with specific parameters. A total of 32 traits were included in this study, and median and inter-quartile range (Iqr) were calculated for each trait at the bird level. In co-expression networks, genes

are seen as “nodes” and “edges” (or connection strengths) between nodes are determined by the pairwise correlations between gene expression profiles.

Before network construction, we calculated the RMA normalized expression of the CEL files using the “justRMA” function in the “affy” R package v1.66.0 (Gautier et al., 2004). We followed the suggestion of the authors of the WGCNA R package using the “collapseRows” function in the WGCNA R package to aggregate gene expression data to gene level (Miller et al., 2011). We constructed a signed hybrid network composed of all HVC samples (n = 39, Table 1) using the “adjacency” function (type: “signed hybrid”). The soft thresholding power for the construction of the adjacency matrix was set at 6 judging from the fitted curves calculated by the “pickSoftThreshold” function. The adjacency value has a range from zero to one. The calculated adjacency matrix was fed to the “TOMsimilarity” function to calculate the topological overlap matrix. Then, we used the “cutreeDynamic” function to cluster genes into modules (sub-networks within the overall network) based on the topological overlap matrix (the “TOMsimilarity” function). We used a minimum module size of 100 genes and the “deepSplit” was set to four. We merged similar modules using the “mergeCloseModules” function (“cutHeight” was set to 20%). Module Eigengenes is the first principal component of a module’s gene expression profile, a method of summarizing an entire module in one vector (Burkett et al., 2018; Langfelder and Horvath, 2008, 2012). We calculated Module Eigengenes using the “moduleEigengenes” function and calculated the correlation matrix between the Module Eigengenes and the traits using the “cor” function (Pearson) in R (Team, 2020). Gene significance is the Pearson correlation between a gene’s expression profile and the traits (Burkett et al., 2018; Langfelder and Horvath, 2008, 2012). The overall network connectivity, intramodular, and intermodular connectivity were calculated using the “intramodularConnectivity” function in the WGCNA package. The adjacency matrix was exported using the “exportNetworkToCytoscape” function with a cutoff of 0.5 and was used for extracting the direct neighbors of *SP8*. The interactions between *SP8* and its direct neighbors were evaluated using the

Search Tool for the Retrieval of Interacting Genes/Proteins database (STRING, v10.5 (Szklarczyk et al., 2015)). The interactions with moderate confidence were retained (combined score greater than 0.4) and were visualized using Cytoscape environment v3.5.1 (Bindea et al., 2009; Shannon et al., 2003).

Experimental design and statistical analysis.

All statistical analyses were performed in R (Team, 2020). For statistical comparisons of plasma androgen levels, song features, and quantification of RNAScope® *in situ* hybridization, we used linear mixed-effect models to analyze the fixed effects using the packages 'lme4' (Bates et al., 2014) and 'arm' (Gelman and Su, 2018) in a Bayesian framework with non-informative priors. We assumed a Gaussian error distribution and confirmed that model assumptions were met by visual inspection of model residuals. Plasma androgen levels, daily song rate, song length, and syllable repetition rate were log-transformed, while the normalized stained HVC areas (RNAScope®) were square root transformed. Subsequently, we simulated 10,000 times the estimates from the joint posterior distribution of the model parameters using the 'sim' function and extracted the 95% credible intervals (CrI) of the mean of the simulated values, which represent the uncertainty of the estimates (Gelman and Hill, 2006). We considered an effect to be statistically meaningful when the estimated CrI did not include zero or when the posterior probability of the mean of the difference between compared estimates was higher than 0.95 (for more details on statistical inference see (Korner-Nievergelt et al., 2015)). Linear mixed-effect models, model estimates, and posterior probability of comparisons were given in Supplementary File 2 and Supplementary File 3. For visualization, we plotted the predicted estimate from the models, the 2.5% and 97.5% CrI, as well as the raw data. Statistically meaningful differences between compared groups can be inferred if the CrI of one group does not overlap with the mean estimate of the other.

Materials availability statement.

The datasets presented in this study can be found in online repositories. The microarray CEL files are available on NCBI's Gene Expression Omnibus (https://www.ncbi.nlm.nih.gov/geo/query/acc.cgi?acc=GSE118522). The custom MATLAB sound analysis program, Multi_Channel_Analyser (MCA) is available in GitLab (https://doi.org/10.5281/zenodo.1489098). The processed microarray data, plasma androgen levels, HVC volume measurements, and song parameters were deposited on Dryad (doi:10.5061/dryad.5hqbzkh8c). All scripts used for analysis and visualization are available on GitHub (https://github.com/maggieMCKO/TimeLapseTestoFemaleCanary).

Acknowledgments.

We thank Dr. Stefan Leitner for providing breeding canaries, Roswitha Brighton and David Witkowski for maintaining the colony, and Dr. Wolfgang Goymann and Monika Trappschuh for radioimmunoassay of plasma androgens. Furthermore, we express our appreciation to Drs. Maude Baldwin, Falk Dittrich, Vincent Van Meir, and Michiel Vellema for their comments on previous versions of this manuscript and to the International Max Planck Research School for Organismal Biology for training and support.

Competing interests

The authors declare no competing financial interests.

Figure legends

Fig. 1. Testosterone implantation increased blood androgen levels, affects the HVC morphology, and affects the song syntax of adult female canaries. A, illustration of experimental procedures. A blood sample was taken from each bird before implantation (blue shaded box) and at the time of sacrifice (orange vertical bars). CON: birds treated with empty implants; T: birds treated with testosterone-filled implants for 1 hour (T1h), 3hours (T3h), eight hours (T8h), 3 days (T3d), seven days (T7d), and fourteen days (T14d). **B**, testosterone implantation significantly increased the androgen concentrations in blood plasma at all time points. Each color-coded dot represents a measurement, before (blue) and after (orange) implantation. The black dots indicate the predicted estimates of the linear mixed-effects models, and the vertical orange bars indicate the 95% credibility intervals (CrI) of the predicted estimates. See Supplementary Files 2 and 3 for the values of the linear mixed-effects models and posterior probabilities. **C**, the daily singing activity (percentage of time spent singing within nine hours in a day) of T7d and T14d groups significantly increased twice on day 2 and day 10 (see also **Figure 1 – Figure supplement 3**). Each grey dot is one bird. **D**, Song length in seconds (s) of T7d and T14d groups. Song length significantly increased daily until day 7 and further increased on day 11. **E**, the number of syllables per song of the T7d and T14d groups increased significantly daily after implantation. **F**, syllable repetition rate as syllables per second (syl/s) of the T7d and T14d groups significantly increased on day 2 and day 9. In D-F, each gray dot represents a measurement originating from one song. In C-F, black dots indicate the predicted estimates of the linear mixed-effects models, and vertical orange bars indicate the 95% credibility intervals (CrI) of the predicted estimates. See **Supplementary File 2** and **Supplementary File 3** for the estimates of the linear mixed-effects models and the posterior probabilities. **G**, HVC volumes of T14d were significantly different from that of control and T1h groups. The boxes indicate the 25th/50th/75th percentiles (bottom/middle/top bar), and the extent of the whiskers indicates the most extreme values within 1.5 times of the inter-quartile range (IQR) of the hinge. Outliers are labeled in

red. *: Holm-adjusted P-value <0.05 (Kruskal-Wallis rank sum test followed by Dunn's post hoc test). Sample sizes of panel B to G are listed in **Table 1**.

Fig. 2. Testosterone rapidly and persistently altered gene expression patterns in the HVC. A, number of differentially expressed genes in the HVC of testosterone-treated birds compared with controls. The proportions of transcription factors (TF) were indicated in darker orange (upregulated genes) and darker purple (downregulated genes). Already within one hour (T1h) more than 2,500 genes were up- or down-regulated. A massive increase in gene regulation occurred 14 days (T14d) after testosterone implantation. **B,** Only a small number of genes (1.6%) were differentially expressed at all time points. We classified the differentially expressed genes into four classes based on their temporal regulation patterns: 1) genes that are constantly upregulated, 2) genes that are constantly downregulated, 3) dynamically regulated genes that are upregulated or downregulated at all six time points, and 4) genes that are altered in expression at least at one but not at all time points compared with controls (see **Supplementary File 5**). **C**, schematic of the songbird brain with song control areas (white) including the HVC. **D** and **E**, representative photomicrographs of RNAScope *in situ* hybridizations of androgen receptor (*AR*) mRNA in D and 5α-reductase (*SRD5A2*) mRNA in E from controls (CON) and testosterone-treated (T8h resp. T14d) birds. *AR* mRNA expression is increased in the HVC of T14d (B, arrowheads) and *SRD5A2* mRNA is increased in the HVC of T8h animals (C, arrowheads). **F**, testosterone increased the expression of genes in the HVC compared with controls (e.g., *AR*, *SRD5A2*, *UTS2B*), and the expression of many genes differed between time points after testosterone treatment started (e.g., *ALDH1A2*, *HSD17B12*). The *in situ* hybridization data of the five depicted genes confirmed the statistical differences (**Supplementary File 2** and **Supplementary File 3**) observed in the microarray-derived expression measurements (see **Fig. 3**A). Data represent the proportion of the labeled HVC area (RNAscope staining of gene mRNA, see D and E) relative to the total HVC area of that section. Each gray dot represents the value of one HVC

section. Black dots indicate the predicted estimates of the linear mixed-effects models, and vertical orange bars indicate the 95% confidence intervals (CrI) of the predicted estimates. N = 3 birds per group. *ALDH1A2*: aldehyde dehydrogenase 1 family member A2; *AR*: androgen receptor; *HSD17B12*: 17β-hydroxysteroid dehydrogenase; *SRD5A2*: 5α-reductases 2; *UTS2B*: urotensin 2B.

Fig. 3. Testosterone rapidly and persistently altered gene expression patterns in the HVC. A, a heat map showing the expression levels of selected groups of genes during testosterone treatment as compared to the control HVCs ($\log_2$ fold change): genes of gonadal steroid receptor genes (blue), genes with known functions in steroidogenesis (gray), genes involved in testosterone-induced angiogenesis (red), genes involved in neuronal recruitment (green), and the gene encoding transcription factor *SP8* (yellow). Please refer to Figure 3 - Figure Supplement 1 for representative plots showing the bird-level normalized expression levels of *AR*, *HSD17B12*, *SRD5A2*, *ESR1*, *ESR2*, and *SP8*. **B,** GO term enrichment analysis of biological processes involving differentially expressed genes during progressive testosterone action on HVC. The ten most likely GO terms (based on Bonferroni-adjusted P-values) were displayed for each time point and classified into six functional categories. The number of genes observed (cumulative across time points) was presented in a stacked bar graph (see **Supplementary File 8** for full results). Biological processes at the cell and neuron level occur early (1 hour), whereas those at the organs/system level occur late (14 days). **C,** enrichment analyses focusing on genes associated with brain cell types (upper panels) and genes associated with neuronal features (types of neuronal protrusions, genes involved in neurotransmitter biosynthesis, and genes encoding neurotransmitter receptors, lower panels). Gray-filled cells were not significant (Fisher's exact test, P-values corrected by FDR method). Full results are shown in **Supplementary File 9**.

Fig. 4. Identification of key genes relevant for testosterone-driven changes. A, WGCNA, an unsupervised clustering method, grouped testosterone-regulated genes into 14 modules (named by color; numbers indicate the gene count per module) and associated these modules with physiological traits (plasma testosterone concentration (T), body weight in g, brain weight in mg, oviduct weight in mg, HVC volume in mm^3) and song measurements (song rate, song length, syllables per song, syllable repetition rate, syllable length, syllable interval, maximum frequency, Wiener entropy, and song slope). Some gene modules were primarily positively correlated (red cells), while other were mainly negatively correlated with physiological and behavioral parameters. Pearson's r is displayed in a diagram cell (upper value) if the correlation was significant; the lower value represents the Bonferroni-adjusted P-value. **B,** a circos plot displays the entire WGCNA gene coexpression network by positioning the 14 color-coded modules at the outer edge of the circle. Genes within each module are sorted in descending order (clockwise) based on the number of neighbors (height of light orange lines between the outer edge and inner circle of adjacency). SP8, a zinc finger transcription factor, has the highest number of coexpressed genes in the "turquoise" module. Adjacency is represented by blue lines (when SP8 is involved) or gray lines (non-SP8) in the inner circle. **C,** Proteins that might interact with transcription factor SP8 to regulate gene expression in the HVC. Orange circles: transcription factors (TF); green: kinases; blue: actins. The widths of the connections represent the confidence levels (with a minimum of 0.4) given by the STRING database.

Fig. 5. RNAscope *in situ* hybridization reveals co-localization of ESR2 and SP8 mRNAs in a subset of HVC cells. A, RNAscope in situ hybridizations targeting *VGLUT2* (also known as *SLC17A6*, **A1**), *ESR2* (**A2**), and *SP8* (**A3**) mRNAs, with DAPI counterstaining (A1, **A4**). Maximal projection of eight confocal Z planes. Arrows indicate three *SP8*-positive cells which show co-localization with *ESR2*, *two* in *VGLUT2*-negative cells (**B1**, **B2**) and one in a VGLUT2-positive cell

(**B3**), enlarged in B1, B2 and B3 respectively. **B,** Single confocal planes show enlarged cells from dashed squares in panel A.

Fig. 6. The timeline of the differentiation of organizational levels of HVC derived from transcriptome data, HVC morphology measured as volume, and song activity and song syntax measurements after testosterone treatment. The intensities of colors indicate the abundance of the features. Note that the abundance of biological processes related to the circulatory system and neuron development precedes that related to the nervous system development of HVC and precedes the emergence of song. The emergence of a canary typical song pattern coincides with the system development of HVC. HVC morphology (volume) maturated only after about 2 weeks of treatment, coinciding with the most differentiated song patterns uttered by the canaries.

Figures

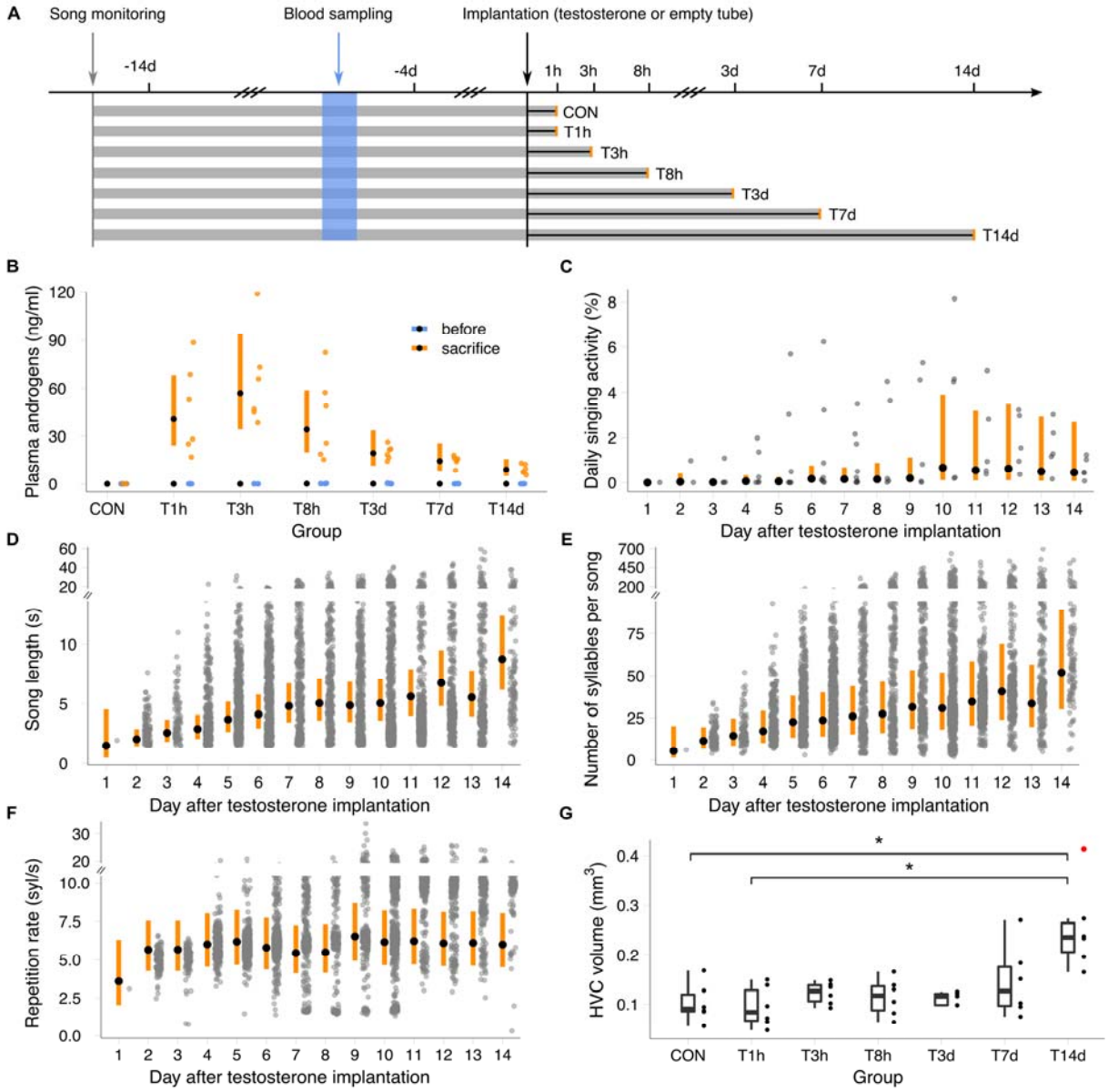

Fig. 1.

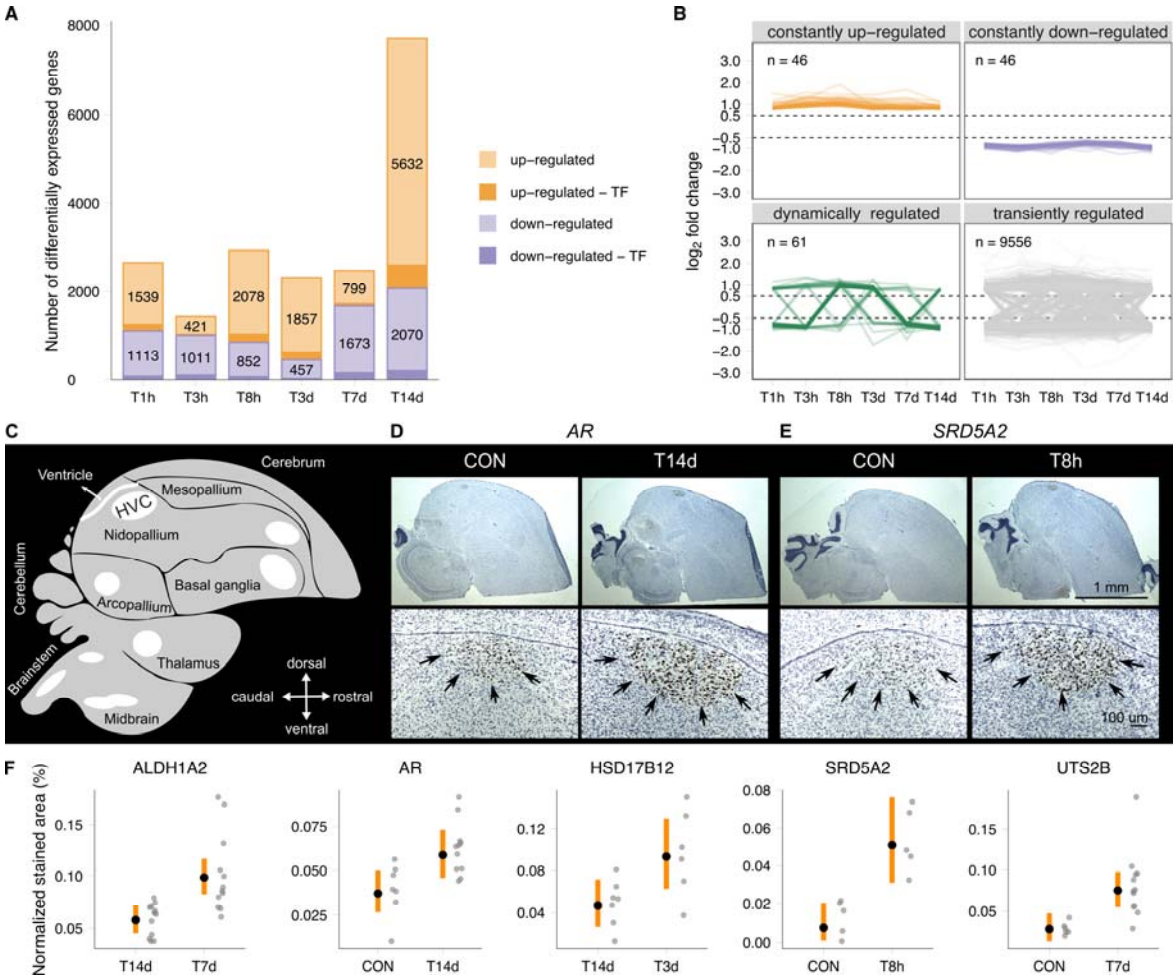
A
Number of differentially expressed genes
8000
6000
4000
2000
0
1539
1113
421
1011
2078
852
1857
457
799
1673
5632
2070
T1h
T3h
T8h
T3d
T7d
T14d
up−regulated
up−regulated − TF
down−regulated
down−regulated − TF
B
constantly up−regulated
constantly down−regulated
dynamically regulated
transiently regulated
n = 46
n = 46
n = 61
n = 9556
log2 fold change
C
Ventricle
Cerebrum
Mesopallium
HVC
Nidopallium
Cerebellum
Basal ganglia
Arcopallium
Brainstem
Thalamus
Midbrain
dorsal
caudal
rostral
ventral
D
AR
CON
T14d
E
SRD5A2
CON
T8h
1 mm
100 um
F
Normalized stained area (%)
ALDH1A2
AR
HSD17B12
SRD5A2
UTS2B
T14d
T7d
CON
T14d
T14d
T3d
CON
T8h
CON
T7d

Fig. 2.

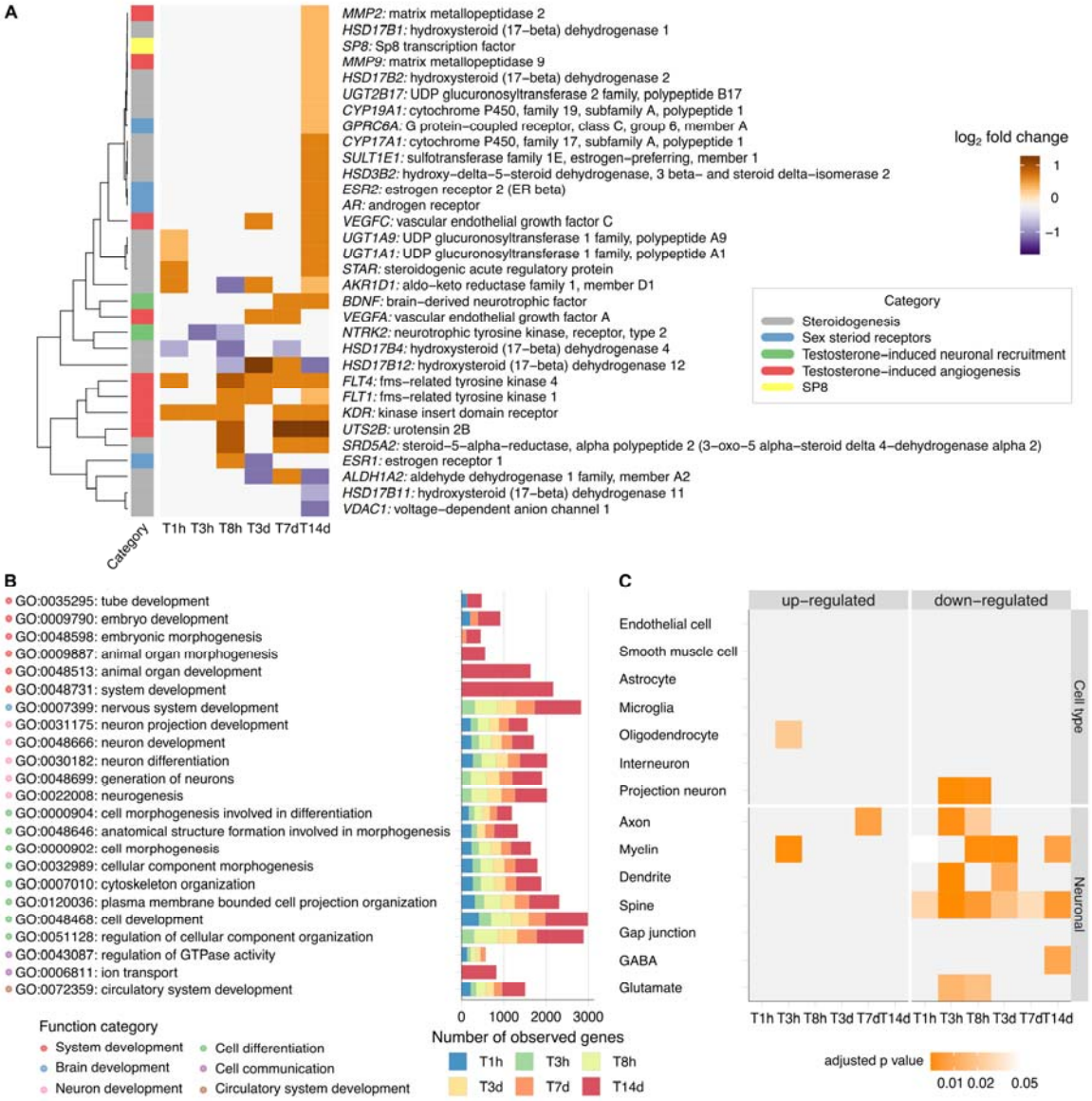
A
MMP2: matrix metallopeptidase 2
HSD17B1: hydroxysteroid (17–beta) dehydrogenase 1
SP8: Sp8 transcription factor
MMP9: matrix metallopeptidase 9
HSD17B2: hydroxysteroid (17–beta) dehydrogenase 2
UGT2B17: UDP glucuronosyltransferase 2 family, polypeptide B17
CYP19A1: cytochrome P450, family 19, subfamily A, polypeptide 1
GPRC6A: G protein–coupled receptor, class C, group 6, member A
CYP17A1: cytochrome P450, family 17, subfamily A, polypeptide 1
SULT1E1: sulfotransferase family 1E, estrogen–preferring, member 1
HSD3B2: hydroxy–delta–5–steroid dehydrogenase, 3 beta– and steroid delta–isomerase 2
ESR2: estrogen receptor 2 (ER beta)
AR: androgen receptor
VEGFC: vascular endothelial growth factor C
UGT1A9: UDP glucuronosyltransferase 1 family, polypeptide A9
UGT1A1: UDP glucuronosyltransferase 1 family, polypeptide A1
STAR: steroidogenic acute regulatory protein
AKR1D1: aldo–keto reductase family 1, member D1
BDNF: brain–derived neurotrophic factor
VEGFA: vascular endothelial growth factor A
NTRK2: neurotrophic tyrosine kinase, receptor, type 2
HSD17B4: hydroxysteroid (17–beta) dehydrogenase 4
HSD17B12: hydroxysteroid (17–beta) dehydrogenase 12
FLT4: fms–related tyrosine kinase 4
FLT1: fms–related tyrosine kinase 1
KDR: kinase insert domain receptor
UTS2B: urotensin 2B
SRD5A2: steroid–5–alpha–reductase, alpha polypeptide 2 (3–oxo–5 alpha–steroid delta 4–dehydrogenase alpha 2)
ESR1: estrogen receptor 1
ALDH1A2: aldehyde dehydrogenase 1 family, member A2
HSD17B11: hydroxysteroid (17–beta) dehydrogenase 11
VDAC1: voltage–dependent anion channel 1
Category
T1h T3h T8h T3d T7d T14d
log2 fold change
1
0
−1
Category
Steroidogenesis
Sex steriod receptors
Testosterone–induced neuronal recruitment
Testosterone–induced angiogenesis
SP8
B
GO:0035295: tube development
GO:0009790: embryo development
GO:0048598: embryonic morphogenesis
GO:0009887: animal organ morphogenesis
GO:0048513: animal organ development
GO:0048731: system development
GO:0007399: nervous system development
GO:0031175: neuron projection development
GO:0048666: neuron development
GO:0030182: neuron differentiation
GO:0048699: generation of neurons
GO:0022008: neurogenesis
GO:0000904: cell morphogenesis involved in differentiation
GO:0048646: anatomical structure formation involved in morphogenesis
GO:0000902: cell morphogenesis
GO:0032989: cellular component morphogenesis
GO:0007010: cytoskeleton organization
GO:0120036: plasma membrane bounded cell projection organization
GO:0048468: cell development
GO:0051128: regulation of cellular component organization
GO:0043087: regulation of GTPase activity
GO:0006811: ion transport
GO:0072359: circulatory system development
0 1000 2000 3000
Number of observed genes
T1h T3h T8h
T3d T7d T14d
Function category
System development
Cell differentiation
Brain development
Cell communication
Neuron development
Circulatory system development
C
up–regulated
down–regulated
Endothelial cell
Smooth muscle cell
Astrocyte
Microglia
Oligodendrocyte
Interneuron
Projection neuron
Axon
Myelin
Dendrite
Spine
Gap junction
GABA
Glutamate
Cell type
Neuronal
T1h T3h T8h T3d T7d T14d T1h T3h T8h T3d T7d T14d
adjusted p value
0.01 0.02 0.05

Fig. 3

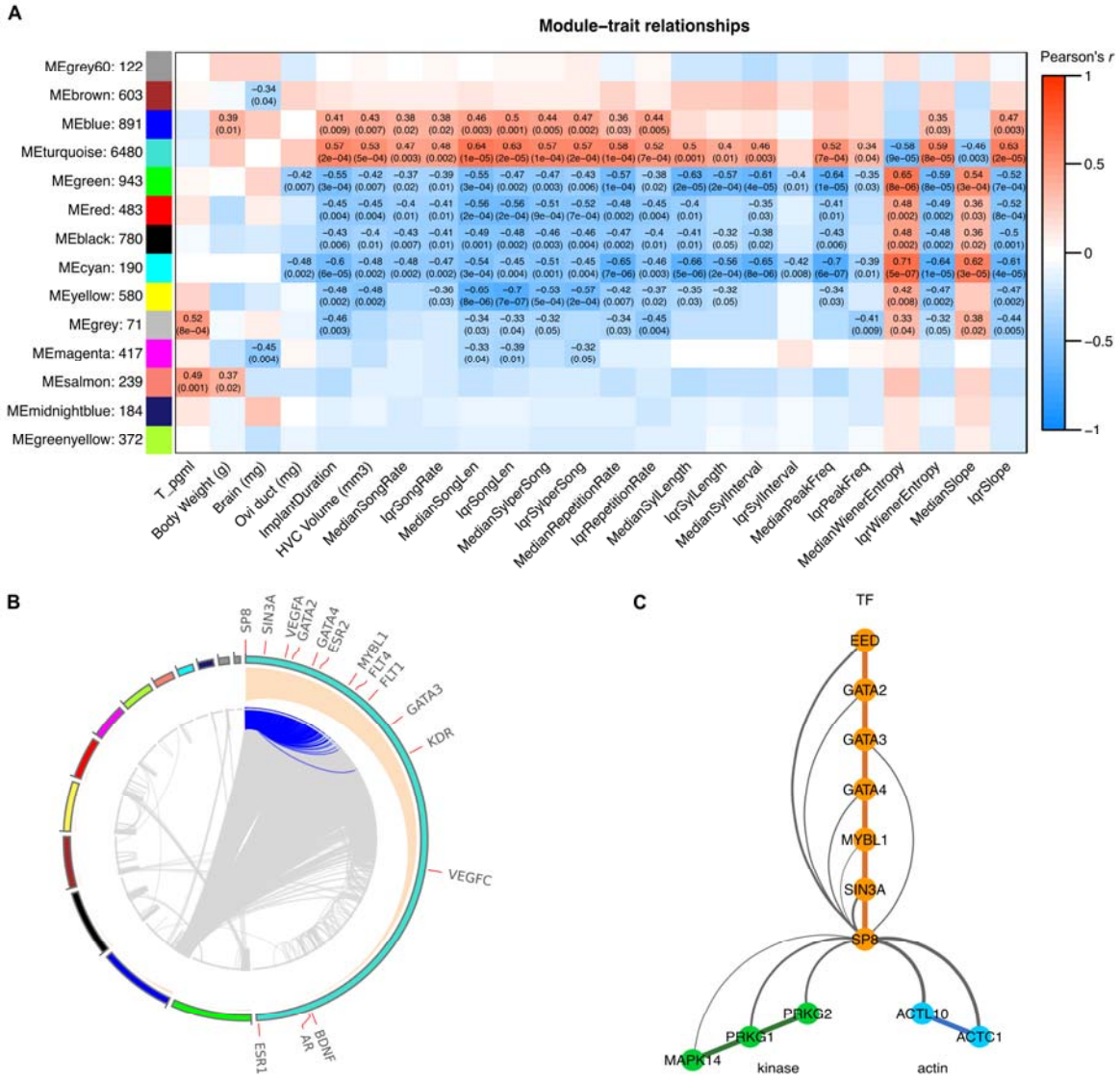
A
Module−trait relationships
MEgrey60: 122
MEbrown: 603
MEblue: 891
MEturquoise: 6480
MEgreen: 943
MEred: 483
MEblack: 780
MEcyan: 190
MEyellow: 580
MEgrey: 71
MEmagenta: 417
MEsalmon: 239
MEmidnightblue: 184
MEgreenyellow: 372
T_pgml
Body Weight (g)
Brain (mg)
Ovi duct (mg)
ImplantDuration
HVC Volume (mm3)
MedianSongRate
IqrSongRate
MedianSongLen
IqrSongLen
MedianSylperSong
IqrSylperSong
MedianRepetitionRate
IqrRepetitionRate
MedianSylLength
IqrSylLength
MedianSylInterval
IqrSylInterval
MedianPeakFreq
IqrPeakFreq
MedianWienerEntropy
IqrWienerEntropy
MedianSlope
IqrSlope
Pearson's r
1
0.5
0
−0.5
−1
B
SP8
SIN3A
VEGFA
GATA2
GATA4
ESR2
MYBL1
FLT4
FLT1
GATA3
KDR
VEGFC
ESR1
AR
BDNF
C
TF
EED
GATA2
GATA3
GATA4
MYBL1
SIN3A
SP8
PRKG2
PRKG1
MAPK14
kinase
ACTL10
ACTC1
actin

Fig. 4

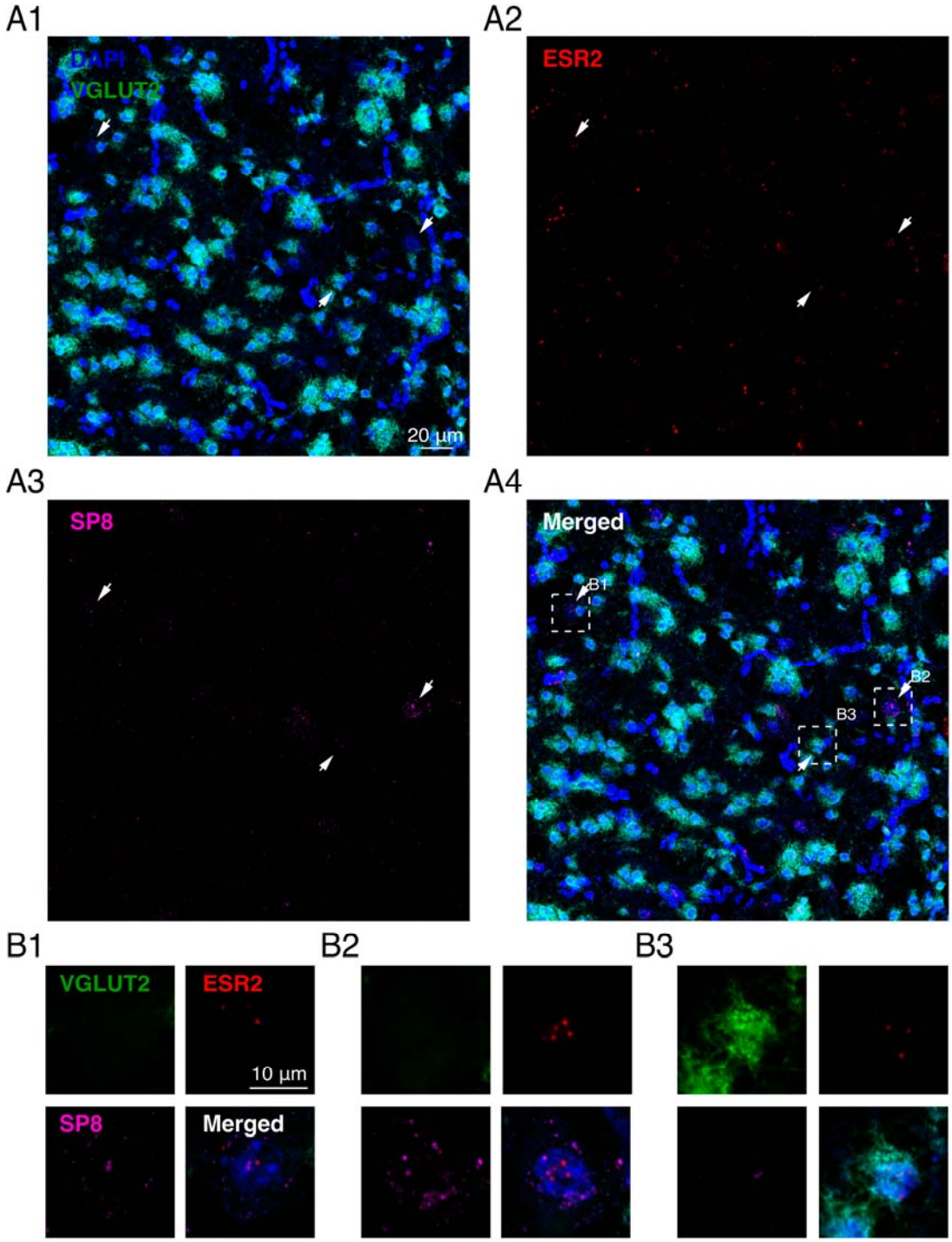
A1
DAPI
VGLUT2
20 µm
A2
ESR2
A3
SP8
A4
Merged
B1
B2
B3
B1
VGLUT2
ESR2
10 µm
SP8
Merged
B2
B3

Fig. 5

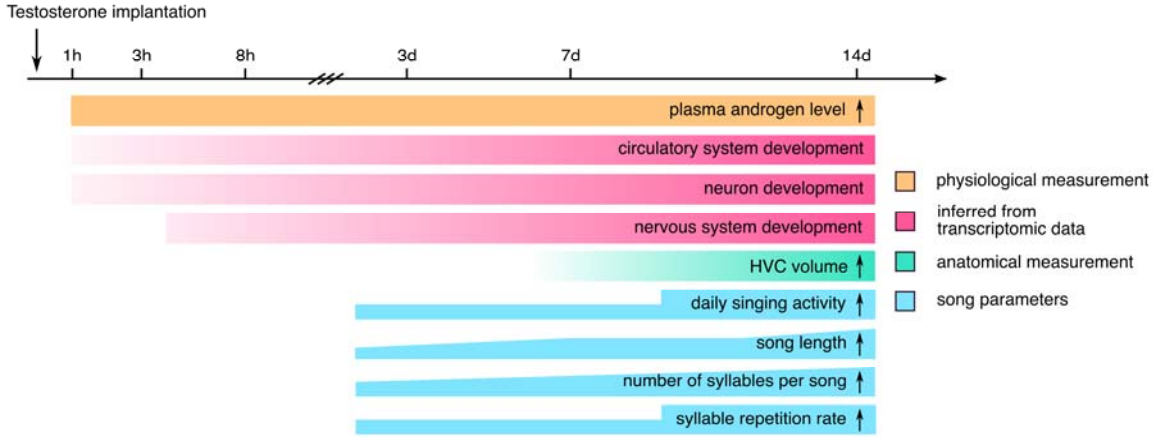
Testosterone implantation
1h
3h
8h
3d
7d
14d
plasma androgen level
circulatory system development
neuron development
nervous system development
HVC volume
daily singing activity
song length
number of syllables per song
syllable repetition rate
physiological measurement
inferred from transcriptomic data
anatomical measurement
song parameters

Fig. 6

References

Alcami, P., Ma, S., Gahr, M., 2021. Telemetry reveals rapid duel-driven song plasticity in a naturalistic social environment. bioRxiv, 803411.

Alcami, P., Totagera, S., Sohnius-Wilhelmi, N., Leitner, S., Grothe, B., Frankl-Vilches, C., Gahr, M., 2021. Extensive GJD2 Expression in the Song Motor Pathway Reveals the Extent of Electrical Synapses in the Songbird Brain. Biology 10, 1099.

Alliende, J., Giret, N., Pidoux, L., Del Negro, C., Leblois, A., 2017. Seasonal plasticity of song behavior relies on motor and syntactic variability induced by a basal ganglia-forebrain circuit. Neuroscience 359, 49-68.

Apfelbeck, B., Kiefer, S., Mortega, K.G., Goymann, W., Kipper, S., 2012. Testosterone Affects Song Modulation during Simulated Territorial Intrusions in Male Black Redstarts (Phoenicurus ochruros). PLOS ONE 7, e52009.

Arnold, A.P., Nottebohm, F., Pfaff, D.W., 1976. Hormone concentrating cells in vocal control and other areas of the brain of the zebra finch (Poephila guttata). J Comp Neurol 165, 487-511.

Ashburner, M., Ball, C.A., Blake, J.A., Botstein, D., Butler, H., Cherry, J.M., Davis, A.P., Dolinski, K., Dwight, S.S., Eppig, J.T., Harris, M.A., Hill, D.P., Issel-Tarver, L., Kasarskis, A., Lewis, S., Matese, J.C., Richardson, J.E., Ringwald, M., Rubin, G.M., Sherlock, G., 2000. Gene Ontology: tool for the unification of biology. Nature Genetics 25, 25.

Ball, G.F., Auger, C.J., Bernard, D.J., Charlier, T.D., Sartor, J.J., Riters, L.V., Balthazart, J., 2004. Seasonal plasticity in the song control system: multiple brain sites of steroid hormone action and the importance of variation in song behavior. Ann N Y Acad Sci 1016, 586-610.

Ball, G.F., Balthazart, J., 2002. Neuroendocrine mechanisms regulating reproductive cycles and reproductive behavior in birds, Hormones, brain and behavior. Elsevier, pp. 649-XII.

Bao, R., Onishi, K.G., Tolla, E., Ebling, F.J.P., Lewis, J.E., Anderson, R.L., Barrett, P., Prendergast, B.J., Stevenson, T.J., 2019. Genome sequencing and transcriptome analyses of the Siberian hamster hypothalamus identify mechanisms for seasonal energy balance. Proceedings of the National Academy of Sciences 116, 13116-13121.

Basista, M.J., Elliott, K.C., Wu, W., Hyson, R.L., Bertram, R., Johnson, F., 2014. Independent premotor encoding of the sequence and structure of birdsong in avian cortex. J Neurosci 34, 16821-16834.

Bates, D., Mächler, M., Bolker, B., Walker, S., 2014. Fitting linear mixed-effects models using lme4. arXiv preprint arXiv:1406.5823.

Bell, S.M., Schreiner, C.M., Waclaw, R.R., Campbell, K., Potter, S.S., Scott, W.J., 2003. Sp8 is crucial for limb outgrowth and neuropore closure. Proceedings of the National Academy of Sciences of the United States of America 100, 12195-12200.

Benson, D.A., Karsch-Mizrachi, I., Lipman, D.J., Ostell, J., Wheeler, D.L., 2005. GenBank. Nucleic Acids Research 33, D34-D38.

Bernard, D.J., Bentley, G.E., Balthazart, J., Turek, F.W., Ball, G.F., 1999. Androgen Receptor, Estrogen Receptor α, and Estrogen Receptorβ Show Distinct Patterns of Expression in Forebrain Song Control Nuclei of European Starlings. Endocrinology 140, 4633-4643.

Bindea, G., Mlecnik, B., Hackl, H., Charoentong, P., Tosolini, M., Kirilovsky, A., Fridman, W.-H., Pagès, F., Trajanoski, Z., Galon, J., 2009. ClueGO: a Cytoscape plug-in to decipher functionally grouped gene ontology and pathway annotation networks. Bioinformatics 25, 1091-1093.

Bissegger, S., Martyniuk, C.J., Langlois, V.S., 2014. Transcriptomic profiling in Silurana tropicalis testes exposed to finasteride. General and Comparative Endocrinology 203, 137-145.

Bourdeau, V.r., Desche□nes, J., Métivier, R.l., Nagai, Y., Nguyen, D., Bretschneider, N., Gannon, F., White, J.H., Mader, S., 2004. Genome-Wide Identification of High-Affinity Estrogen Response Elements in Human and Mouse. Molecular Endocrinology 18, 1411-1427.

Burkett, Z.D., Day, N.F., Kimball, T.H., Aamodt, C.M., Heston, J.B., Hilliard, A.T., Xiao, X., White, S.A., 2018. FoxP2 isoforms delineate spatiotemporal transcriptional networks for vocal learning in the zebra finch. eLife 7, e30649.

Byers, J., Hebets, E., Podos, J., 2010. Female mate choice based upon male motor performance. Animal Behaviour 79, 771-778.

Carrier, N., Saland, S.K., Duclot, F., He, H., Mercer, R., Kabbaj, M., 2015. The Anxiolytic and Antidepressant-like Effects of Testosterone and Estrogen in Gonadectomized Male Rats. Biol Psychiatry 78, 259-269.

Cartharius, K., Frech, K., Grote, K., Klocke, B., Haltmeier, M., Klingenhoff, A., Frisch, M., Bayerlein, M., Werner, T., 2005. MatInspector and beyond: promoter analysis based on transcription factor binding sites. Bioinformatics 21, 2933-2942.

Catchpole, C.K., Slater, P.J.B., 2018. Bird Song: Biological Themes and Variations, 2nd ed.

Celec, P., Ostatníková, D., Hodosy, J., 2015. On the effects of testosterone on brain behavioral functions. Frontiers in Neuroscience 9.

Cheviron, Z.A., Swanson, D.L., 2017. Comparative Transcriptomics of Seasonal Phenotypic Flexibility in Two North American Songbirds. Integr Comp Biol 57, 1040-1054.

Choe, H.N., Tewari, J., Zhu, K.W., Davenport, M., Matsunami, H., Jarvis, E.D., 2021. Estrogen and sex-dependent loss of the vocal learning system in female zebra finches. Hormones and Behavior 129, 104911.

Cohen, C.D., Lindenmeyer, M.T., Eichinger, F., Hahn, A., Seifert, M., Moll, A.G., Schmid, H., Kiss, E., Grone, E., Grone, H.J., Kretzler, M., Werner, T., Nelson, P.J., 2008. Improved elucidation of biological processes linked to diabetic nephropathy by single probe-based microarray data analysis. PLoS One 3, e2937.

Colquitt, B.M., Merullo, D.P., Konopka, G., Roberts, T.F., Brainard, M.S., 2021. Cellular transcriptomics reveals evolutionary identities of songbird vocal circuits. Science 371, eabd9704.

Consortium, T.G.O., 2017. Expansion of the Gene Ontology knowledgebase and resources. Nucleic Acids Research 45, D331-D338.

Consortium, T.U., 2015. UniProt: a hub for protein information. Nucleic Acids Research 43, D204-D212.

Cornez, G., Shevchouk, O.T., Ghorbanpoor, S., Ball, G.F., Cornil, C.A., Balthazart, J., 2020. Testosterone stimulates perineuronal nets development around parvalbumin cells in the adult canary brain in parallel with song crystallization. Horm Behav 119, 104643.

de Bournonville, M.P., de Bournonville, C., Vandries, L.M., Nys, G., Fillet, M., Ball, G.F., Balthazart, J., Cornil, C.A., 2021. Rapid changes in brain estrogen concentration during male sexual behavior are site and stimulus specific. Sci Rep 11, 20130.

Dittrich, F., Ramenda, C., Grillitsch, D., Frankl-Vilches, C., Ko, M.C., Hertel, M., Goymann, W., Ter Maat, A., Gahr, M., 2014. Regulatory mechanisms of testosterone-stimulated song in the sensorimotor nucleus HVC of female songbirds. BMC Neurosci 15, 128.

Dopico, X.C., Evangelou, M., Ferreira, R.C., Guo, H., Pekalski, M.L., Smyth, D.J., Cooper, N., Burren, O.S., Fulford, A.J., Hennig, B.J., Prentice, A.M., Ziegler, A.G., Bonifacio, E., Wallace, C., Todd, J.A., 2015. Widespread seasonal gene expression reveals annual differences in human immunity and physiology. Nat Commun 6, 7000.

Drăgănoiu, T.I., Nagle, L., Kreutzer, M., 2002. Directional female preference for an exaggerated male trait in canary (Serinusanaria) song. Proceedings of the Royal Society of London. Series B: Biological Sciences 269, 2525.

Edgar, R., Domrachev, M., Lash, A., 2002. Gene Expression Omnibus: NCBI gene expression and hybridization array data repository. Nucleic Acids Res 30, 207 - 210.

Faber-Hammond, J., Samanta, M.P., Whitchurch, E.A., Manning, D., Sisneros, J.A., Coffin, A.B., 2015. Saccular Transcriptome Profiles of the Seasonal Breeding Plainfin Midshipman Fish (Porichthys notatus), a Teleost with Divergent Sexual Phenotypes. PLoS One 10, e0142814.

Farcas, A.M., Nagarajan, S., Cosulich, S., Carroll, J.S., 2020. Genome-Wide Estrogen Receptor Activity in Breast Cancer. Endocrinology 162.

Félix, A.S., Cardoso, S.D., Roleira, A., Oliveira, R.F., 2020. Forebrain Transcriptional Response to Transient Changes in Circulating Androgens in a Cichlid Fish. G3 (Bethesda) 10, 1971-1982.

Flicek, P., Amode, M.R., Barrell, D., Beal, K., Billis, K., Brent, S., Carvalho-Silva, D., Clapham, P., Coates, G., Fitzgerald, S., Gil, L., Girón, C.G., Gordon, L., Hourlier, T., Hunt, S., Johnson, N., Juettemann, T., Kähäri, A.K., Keenan, S., Kulesha, E., Martin, F.J., Maurel, T., McLaren, W.M., Murphy, D.N., Nag, R., Overduin, B., Pignatelli, M., Pritchard, B., Pritchard, E., Riat, H.S., Ruffier, M., Sheppard, D., Taylor, K., Thormann, A., Trevanion, S.J., Vullo, A., Wilder, S.P., Wilson, M., Zadissa, A., Aken, B.L., Birney, E., Cunningham, F., Harrow, J., Herrero, J., Hubbard, T.J.P., Kinsella, R., Muffato, M., Parker, A., Spudich, G., Yates, A., Zerbino, D.R., Searle, S.M.J., 2014. Ensembl 2014. Nucleic Acids Research 42, D749-D755.

Forlano, P.M., Sisneros, J.A., Rohmann, K.N., Bass, A.H., 2015. Neuroendocrine control of seasonal plasticity in the auditory and vocal systems of fish. Front Neuroendocrinol 37, 129-145.

Frankl-Vilches, C., Gahr, M., 2017. Androgen and estrogen sensitivity of bird song: a comparative view on gene regulatory levels. Journal of Comparative Physiology A.

Frankl-Vilches, C., Kuhl, H., Werber, M., Klages, S., Kerick, M., Bakker, A., de Oliveira, E.H., Reusch, C., Capuano, F., Vowinckel, J., Leitner, S., Ralser, M., Timmermann, B., Gahr, M., 2015. Using the canary genome to decipher the evolution of hormone-sensitive gene regulation in seasonal singing birds. Genome Biol 16, 19.

Fuentes, N., Silveyra, P., 2019. Estrogen receptor signaling mechanisms. Adv Protein Chem Struct Biol 116, 135-170.

Fusani, L., Metzdorf, R., Hutchison, J., Gahr, M., 2003. Aromatase inhibition affects testosterone-induced masculinization of song and the neural song system in female canaries. J Neurobiol 54, 370 - 379.

Gaborieau, E., Hurtado-Chong, A., Fernández, M., Azim, K., Raineteau, O., 2018. A dual role for the transcription factor Sp8 in postnatal neurogenesis. Scientific Reports 8, 14560.

Gahr, M., 1990a. Delineation of a brain nucleus: comparisons of cytochemical, hodological, and cytoarchitectural views of the song control nucleus HVc of the adult canary. J Comp Neurol 294, 30-36.

Gahr, M., 1990b. Localization of androgen receptors and estrogen receptors in the same cells of the songbird brain. Proc Natl Acad Sci U S A 87, 9445 - 9448.

Gahr, M., 2001. Distribution of sex steroid hormone receptors in the avian brain: Functional implications for neural sex differences and sexual behaviors. Microscopy Research and Technique 55, 1-11.

Gahr, M., 2004. Hormone-dependent neural plasticity in the juvenile and adult song system: what makes a successful male? Ann N Y Acad Sci 1016, 684-703.

Gahr, M., 2014. How Hormone-Sensitive Are Bird Songs And What Are The Underlying Mechanisms? Acta Acustica United with Acustica 100, 705-718.

Gahr, M., 2020. Seasonal hormone fluctuations and song structure of birds. Coding strategies in vertebrate acoustic communication, 163-201.

Gahr, M., Garcia-Segura, L.M., 1996. Testosterone-dependent increase of gap-junctions in HVC neurons of adult female canaries. Brain Research 712, 69-73.

Gahr, M., Metzdorf, R., 1997. Distribution and dynamics in the expression of androgen and estrogen receptors in vocal control systems of songbirds. Brain Res Bull 44, 509 - 517.

Gahr, M., Wild, J.M., 1997. Localization of androgen receptor mRNA-containing cells in avian respiratory-vocal nuclei: an in situ hybridization study. J Neurobiol 33, 865-876.

Gardner, M., 1978. White and brown music, fractal curves and one-over-f fluctuations. Scientific American 238, 16-33.

Gautier, L., Cope, L., Bolstad, B.M., Irizarry, R.A., 2004. affy—analysis of Affymetrix GeneChip data at the probe level. Bioinformatics 20, 307-315.

Gelman, A., Hill, J., 2006. Data analysis using regression and multilevel/hierarchical models. Cambridge university press.

Gelman, A., Su, Y.-S., 2018. arm: Data Analysis Using Regression and Multilevel/Hierarchical Models, 1.10-1 ed, pp. R package version 1.10-11.

Gisiger, T., 2001. Scale invariance in biology: coincidence or footprint of a universal mechanism? Biological Reviews 76, 161-209.

Godsave, S.F., Lohmann, R., Vloet, R.P., Gahr, M., 2002. Androgen receptors in the embryonic zebra finch hindbrain suggest a function for maternal androgens in perihatching survival. J Comp Neurol 453, 57-70.

Goldin, M.A., Alonso, L.M., Alliende, J.A., Goller, F., Mindlin, G.B., 2013. Temperature induced syllable breaking unveils nonlinearly interacting timescales in birdsong motor pathway. PLoS One 8, e67814.

Goldman, S., Nottebohm, F., 1983. Neuronal production, migration, and differentiation in a vocal control nucleus in the adult female canary brain. Proc Natl Acad Sci U S A 80, 2390.

Goymann, W., Möstl, E., Gwinner, E., 2002. Non-invasive methods to measure androgen metabolites in excrements of European stonechats, Saxicola torquata rubicola. General and Comparative Endocrinology 129, 80-87.

Guh, Y.-J., Tamai, T.K., Yoshimura, T., 2019. The underlying mechanisms of vertebrate seasonal reproduction. Proceedings of the Japan Academy, Series B 95, 343-357.

Guillemette, C., 2003. Pharmacogenomics of human UDP-glucuronosyltransferase enzymes. The Pharmacogenomics Journal 3, 136.

Hahnloser, R.H.R., Kozhevnikov, A.A., Fee, M.S., 2002. An ultra-sparse code underliesthe generation of neural sequences in a songbird. Nature 419, 65-70.

Hartley, R.S., Chinn, M.S., Ullrich, N.F.E., 1997. Left Syringeal Dominance in Testosterone-Treated Female Canaries. Neurobiology of Learning and Memory 67, 248-253.

Hartog, T., Dittrich, F., Pieneman, A., Jansen, R., Frankl-Vilches, C., Lessmann, V., 2009. Brain-derived neurotrophic factor signaling in the HVC is required for testosterone-induced song of female canaries. J Neurosci 29, 15511 - 15519.

Hausberger, M., Henry, L., Richard, M.A., 1995. Testosterone-induced Singing in Female European Starlings (Sturnus vulgaris). Ethology 99, 193-208.

Herrick, E.H., Harris, J.O., 1957. Singing Female Canaries. Science 125, 1299-1300.

Huang, D.W., Sherman, B.T., Lempicki, R.A., 2008. Systematic and integrative analysis of large gene lists using DAVID bioinformatics resources. Nature Protocols 4, 44-57.

Huang, D.W., Sherman, B.T., Lempicki, R.A., 2009. Bioinformatics enrichment tools: paths toward the comprehensive functional analysis of large gene lists. Nucleic Acids Research 37, 1-13.

Jarvis, E.D., Nottebohm, F., 1997. Motor-driven gene□expression. Proceedings of the National Academy of Sciences 94, 4097-4102.

Jennings, K.J., de Lecea, L., 2020. Neural and Hormonal Control of Sexual Behavior. Endocrinology 161.

Jia, Y., Castellanos, J., Wang, C., Sinha-Hikim, I., Lue, Y., Swerdloff, R.S., Sinha-Hikim, A.P., 2009. Mitogen-activated protein kinase signaling in male germ cell apoptosis in the rat. Biol Reprod 80, 771-780.

Johnson, F., Bottjer, S.W., 1993. Hormone-induced changes in identified cell populations of the higher vocal center in male canaries. Journal of Neurobiology 24, 400-418.

Johnson, F., Bottjer, S.W., 1995. Differential estrogen accumulation among populations of projection neurons in the higher vocal center of male canaries. Journal of Neurobiology 26, 87-108.

Kilkenny, C., Browne, W.J., Cuthill, I.C., Emerson, M., Altman, D.G., 2010. Improving bioscience research reporting: the ARRIVE guidelines for reporting animal research. PLoS Biol 8, e1000412.

Kim, D.-H., Lilliehook, C., Roides, B., Chen, Z., Chang, M., Mobashery, S., Goldman, S.A., 2008. Testosterone-Induced Matrix Metalloproteinase Activation Is a Checkpoint for Neuronal Addition to the Adult Songbird Brain. The Journal of Neuroscience 28, 208.

Ko, M.-C., Frankl-Vilches, C., Bakker, A., Gahr, M., 2021. The Gene Expression Profile of the Song Control Nucleus HVC Shows Sex Specificity, Hormone Responsiveness, and Species Specificity Among Songbirds. Frontiers in Neuroscience 15.

Ko, M.-C., Van Meir, V., Vellema, M., Gahr, M., 2020. Characteristics of song, brain-anatomy and blood androgen levels in spontaneously singing female canaries. Hormones and Behavior 117, 104614.

Korner-Nievergelt, F., Roth, T., Von Felten, S., Guélat, J., Almasi, B., Korner-Nievergelt, P., 2015. Bayesian data analysis in ecology using linear models with R, BUGS, and Stan. Academic Press.

Langfelder, P., Horvath, S., 2008. WGCNA: an R package for weighted correlation network analysis. BMC Bioinformatics 9, 1-13.

Langfelder, P., Horvath, S., 2012. Fast R Functions for Robust Correlations and Hierarchical Clustering. Journal of statistical software 46, i11.

Larson, T.A., Lent, K.L., Bammler, T.K., MacDonald, J.W., Wood, W.E., Caras, M.L., Thatra, N.M., Budzillo, A., Perkel, D.J., Brenowitz, E.A., 2015. Network analysis of microRNA and mRNA seasonal dynamics in a highly plastic sensorimotor neural circuit. BMC Genomics 16, 905.

Limame, R., de Beeck, K.O., Lardon, F., Wever, O.D., Pauwels, P., 2014. Krüppel-like factors in cancer progression: three fingers on the steering wheel. Oncotarget 5, 29-48.

Limbourg, F.P., Takeshita, K., Radtke, F., Bronson, R.T., Chin, M.T., Liao, J.K., 2005. Essential role of endothelial Notch1 in angiogenesis. Circulation 111, 1826-1832.

Long, M.A., Fee, M.S., 2008. Using temperature to analyse temporal dynamics in the songbird motor pathway. Nature 456, 189-194.

Louissaint, A., Rao, S., Leventhal, C., Goldman, S.A., 2002. Coordinated Interaction of Neurogenesis and Angiogenesis in the Adult Songbird Brain. Neuron 34, 945-960.

Lovell, P.V., Carleton, J.B., Mello, C.V., 2013. Genomics analysis of potassium channel genes in songbirds reveals molecular specializations of brain circuits for the maintenance and production of learned vocalizations. BMC Genomics 14, 470.

Madison, F.N., Rouse, M.L., Jr., Balthazart, J., Ball, G.F., 2015. Reversing song behavior phenotype: Testosterone driven induction of singing and measures of song quality in adult male and female canaries (Serinus canaria). Gen Comp Endocrinol 215, 61-75.

Marynick, S.P., Havens, W.W., 2nd, Ebert, M.H., Loriaux, D.L., 1976. Studies on the transfer of steroid hormones across the blood-cerebrospinal fluid barrier in the Rhesus Monkey. Endocrinology 99, 400-405.

Metzdorf, R., Gahr, M., Fusani, L., 1999. Distribution of aromatase, estrogen receptor, and androgen receptor mRNA in the forebrain of songbirds and nonsongbirds. J Comp Neurol 407, 115-129.

Michels, G., Hoppe, U.C., 2008. Rapid actions of androgens. Front Neuroendocrinol 29, 182-198.

Migaud, M., Butrille, L., Batailler, M., 2015. Seasonal regulation of structural plasticity and neurogenesis in the adult mammalian brain: focus on the sheep hypothalamus. Front Neuroendocrinol 37, 146-157.

Miller, J.A., Cai, C., Langfelder, P., Geschwind, D.H., Kurian, S.M., Salomon, D.R., Horvath, S., 2011. Strategies for aggregating gene expression data: The collapseRows R function. BMC Bioinformatics 12, 322.

Morey, J.S., Neely, M.G., Lunardi, D., Anderson, P.E., Schwacke, L.H., Campbell, M., Van Dolah, F.M., 2016. RNA-Seq analysis of seasonal and individual variation in blood transcriptomes of healthy managed bottlenose dolphins. BMC Genomics 17, 720.

Nottebohm, F., 1980. Testosterone triggers growth of brain vocal control nuclei in adult female canaries. Brain Res 189, 429-436.

Nottebohm, F., 1981. A brain for all seasons: cyclical anatomical changes in song control nuclei of the canary brain. Science 214, 1368.

Nottebohm, F., Nottebohm, M.E., Crane, L., 1986. Developmental and seasonal changes in canary song and their relation to changes in the anatomy of song-control nuclei. Behavioral and neural biology 46, 445-471.

Nottebohm, F., Stokes, T.M., Leonard, C.M., 1976. Central control of song in the canary, Serinus canarius. The Journal of Comparative Neurology 165, 457-486.

Ouzzine, M., Gulberti, S., Ramalanjaona, N., Magdalou, J., Fournel-Gigleux, S., 2014. The UDP-glucuronosyltransferases of the blood-brain barrier: their role in drug metabolism and detoxication. Frontiers in Cellular Neuroscience 8.

Pan, W., Lin, J., Le, C.T., 2002. How many replicates of arrays are required to detect gene expression changes in microarray experiments? A mixture model approach. Genome Biology 3, research0022.0021.

Pesch, A., Güttinger, H.-R., 1985. Der Gesang des weiblichen Kanarienvogels. Journal für Ornithologie 126, 108-110.

Peterson, M.P., Rosvall, K.A., Choi, J.H., Ziegenfus, C., Tang, H., Colbourne, J.K., Ketterson, E.D., 2013. Testosterone affects neural gene expression differently in male and female juncos: a role for hormones in mediating sexual dimorphism and conflict. PLoS One 8, e61784.

Pi, M., Parrill, A.L., Quarles, L.D., 2010. GPRC6A Mediates the Non-genomic Effects of Steroids. Journal of Biological Chemistry 285, 39953-39964.

Pihlajamaa, P., Sahu, B., Jänne, O.A., 2015. Determinants of Receptor- and Tissue-Specific Actions in Androgen Signaling. Endocrine Reviews 36, 357-384.

Pihlajamaa, P., Sahu, B., Lyly, L., Aittomäki, V., Hautaniemi, S., Jänne, O.A., 2014. Tissue-specific pioneer factors associate with androgen receptor cistromes and transcription programs. The EMBO Journal 33, 312-326.

Quandt, K., Frech, K., Karas, H., Wingender, E., Werner, T., 1995. Matlnd and Matlnspector: new fast and versatile tools for detection of consensus matches in nucleotide sequence data. Nucleic Acids Research 23, 4878-4884.

Quintela, T., Marcelino, H., Gonçalves, I., Patriarca, F.M., Santos, C.R.A., 2015. Gene expression profiling in the hippocampus of orchidectomized rats. J Mol Neurosci 55, 198-205.

Quispe, R., Trappschuh, M., Gahr, M., Goymann, W., 2015. Towards more physiological manipulations of hormones in field studies: comparing the release dynamics of three kinds of testosterone implants, silastic tubing, time-release pellets and beeswax. Gen Comp Endocrinol 212, 100-105.

Rasika, S., Alvarez-Buylla, A., Nottebohm, F., 1999. BDNF mediates the effects of testosterone on the survival of new neurons in an adult brain. Neuron 22, 53-62.

Rasika, S., Nottebohm, F., Alvarez-Buylla, A., 1994. Testosterone increases the recruitment and/or survival of new high vocal center neurons in adult female canaries. Proc Natl Acad Sci U S A 91, 7854-7858.

Reményi, A., Schöler, H.R., Wilmanns, M., 2004. Combinatorial control of gene expression. Nature Structural &Amp; Molecular Biology 11, 812.

Riebel, K., Odom, K.J., Langmore, N.E., Hall, M.L., 2019. New insights from female bird song: towards an integrated approach to studying male and female communication roles. Biology Letters 15, 20190059.

Riters, L.V., Eens, M., Pinxten, R., Duffy, D.L., Balthazart, J., Ball, G.F., 2000. Seasonal changes in courtship song and the medial preoptic area in male European starlings (Sturnus vulgaris). Horm Behav 38, 250-261.

Rueden, C.T., Schindelin, J., Hiner, M.C., DeZonia, B.E., Walter, A.E., Arena, E.T., Eliceiri, K.W., 2017. ImageJ2: ImageJ for the next generation of scientific image data. BMC Bioinformatics 18, 529.

Safe, S., Kim, K., 2008. Non-classical genomic estrogen receptor (ER)/specificity protein and ER/activating protein-1 signaling pathways. Journal of Molecular Endocrinology 41, 263-275.

Sartor, J.J., Balthazart, J., Ball, G.F., 2005. Coordinated and dissociated effects of testosterone on singing behavior and song control nuclei in canaries (Serinus canaria). Horm Behav 47, 467-476.

Schindelin, J., Arganda-Carreras, I., Frise, E., Kaynig, V., Longair, M., Pietzsch, T., Preibisch, S., Rueden, C., Saalfeld, S., Schmid, B., Tinevez, J.-Y., White, D.J., Hartenstein, V., Eliceiri, K., Tomancak, P., Cardona, A., 2012. Fiji: an open-source platform for biological-image analysis. Nature Methods 9, 676.

Schlinger, B., Scanes, C., Randhawa, M., Callard, G., 1984. Distribution of aromatase activity in quail brain (Cc japonica): effects of photoperiod and castration. Journal of Steroid Biochemistry 20, 1571.

Schwartz, C., Andrews, M.T., 2013. Circannual transitions in gene expression: lessons from seasonal adaptations. Curr Top Dev Biol 105, 247-273.

Schwartz, C., Hampton, M., Andrews, M.T., 2013. Seasonal and regional differences in gene expression in the brain of a hibernating mammal. PloS one 8, e58427-e58427.

Shannon, P., Markiel, A., Ozier, O., Baliga, N.S., Wang, J.T., Ramage, D., Amin, N., Schwikowski, B., Ideker, T., 2003. Cytoscape: a software environment for integrated models of biomolecular interaction networks. Genome Res 13, 2498-2504.

Sharma, A., Das, S., Kumar, V., 2019. Transcriptome-wide changes in testes reveal molecular differences in photoperiod-induced seasonal reproductive life-history states in migratory songbirds. Mol Reprod Dev 86, 956-963.

Sharp, P.J., Armstrong, D.G., Moss, R., 1986. Changes in aromatase activity in the neuroendocrine tissues of red grouse (Lagopus lagopus scoticus) in relation to the development of long-day refractoriness. J Endocrinol 108, 129-135.

Shoemaker, H.H., 1939. Effect of Testosterone Propionate on Behavior of the Female Canary. Proceedings of the Society for Experimental Biology and Medicine 41, 299-302.

Snijders, L., van Oers, K., Naguib, M., 2017. Sex-specific responses to territorial intrusions in a communication network: Evidence from radio-tagged great tits. Ecol Evol 7, 918-927.

Stelloo, S., Bergman, A.M., Zwart, W., 2019. Androgen receptor enhancer usage and the chromatin regulatory landscape in human prostate cancers. Endocr Relat Cancer 26, R267-r285.

Sui, S.J.H., Mortimer, J.R., Arenillas, D.J., Brumm, J., Walsh, C.J., Kennedy, B.P., Wasserman, W.W., 2005. oPOSSUM: identification of over-represented transcription factor binding sites in co-expressed genes. Nucleic Acids Research 33, 3154-3164.

Szklarczyk, D., Franceschini, A., Wyder, S., Forslund, K., Heller, D., Huerta-Cepas, J., Simonovic, M., Roth, A., Santos, A., Tsafou, K.P., Kuhn, M., Bork, P., Jensen, L.J., von Mering, C., 2015. STRING v10: protein–protein interaction networks, integrated over the tree of life. Nucleic Acids Research 43, D447-D452.

Takayama, K., Kaneshiro, K., Tsutsumi, S., Horie-Inoue, K., Ikeda, K., Urano, T., Ijichi, N., Ouchi, Y., Shirahige, K., Aburatani, H., Inoue, S., 2007. Identification of novel androgen response genes in prostate cancer cells by coupling chromatin immunoprecipitation and genomic microarray analysis. Oncogene 26, 4453.

Tchernichovski, O., Nottebohm, F., Ho, C.E., Pesaran, B., Mitra, P.P., 2000. A procedure for an automated measurement of song similarity. Anim Behav 59, 1167-1176.

Team, R.C., 2020. R: A language and environment for statistical computing. R Foundation for Statistical Computing [Internet]. Vienna, Austria.

Thompson, C., Meitzen, J., Replogle, K., Drnevich, J., Lent, K., Wissman, A., 2012. Seasonal changes in patterns of gene expression in avian song control brain regions. PLoS One 7, e35119.

Tian, F., Liu, S., Shi, J., Qi, H., Zhao, K., Xie, B., 2019. Transcriptomic profiling reveals molecular regulation of seasonal reproduction in Tibetan highland fish, Gymnocypris przewalskii. BMC genomics 20, 2-2.

Tusher, V.G., Tibshirani, R., Chu, G., 2001. Significance analysis of microarrays applied to the ionizing radiation response. Proc Natl Acad Sci U S A 98, 5116-5121.

Vallet, E., Kreutzer, M., Gahr, M., 1996. Testosterone Induces Sexual Release Quality in the Song of Female Canaries. Ethology 102, 617-628.

Vellema, M., Diales Rocha, M., Bascones, S., Zsebők, S., Dreier, J., Leitner, S., Van der Linden, A., Brewer, J., Gahr, M., 2019. Accelerated redevelopment of vocal skills is preceded by lasting reorganization of the song motor circuitry. eLife 8, e43194.

Vellema, M., van der Linden, A., Gahr, M., 2010. Area-specific migration and recruitment of new neurons in the adult songbird brain. J Comp Neurol 518, 1442-1459.

Voigt, C., Leitner, S., 2008. Seasonality in song behaviour revisited: Seasonal and annual variants and invariants in the song of the domesticated canary (Serinus canaria). Hormones and Behavior 54, 373-378.

Voss, R.F., Clarke, J., 1975. '1/f noise' in music and speech. Nature 258, 317-318.

Waclaw, R.R., Allen, Z.J., Bell, S.M., Erdélyi, F., Szabó, G., Potter, S.S., Campbell, K., 2006. The Zinc Finger Transcription Factor Sp8 Regulates the Generation and Diversity of Olfactory Bulb Interneurons. Neuron 49, 503-516.

Wang, F., Flanagan, J., Su, N., Wang, L.-C., Bui, S., Nielson, A., Wu, X., Vo, H.-T., Ma, X.-J., Luo, Y., 2012. RNAscope: A Novel in Situ RNA Analysis Platform for Formalin-Fixed, Paraffin-Embedded Tissues. The Journal of Molecular Diagnostics 14, 22-29.

Warren, W., Clayton, D., Ellegren, H., Arnold, A., Hillier, L., Kunstner, A., 2010. The genome of a songbird. Nature 464, 757-762.

Watts, H.E., 2020. Seasonal regulation of behaviour: what role do hormone receptors play? Proceedings of the Royal Society B: Biological Sciences 287, 20200722.

Weems, P.W., Goodman, R.L., Lehman, M.N., 2015. Neural mechanisms controlling seasonal reproduction: Principles derived from the sheep model and its comparison with hamsters. Frontiers in Neuroendocrinology 37, 43-51.

Whitney, O., Pfenning, A.R., Howard, J.T., Blatti, C.A., Liu, F., Ward, J.M., Wang, R., Audet, J.N., Kellis, M., Mukherjee, S., Sinha, S., Hartemink, A.J., West, A.E., Jarvis, E.D., 2014. Core and region-enriched networks of behaviorally regulated genes and the singing genome. Science 346, 1256780.

Wickham, H., 2009. ggplot2 - Elegant Graphics for Data Analysis, in: Gentleman, R., Hornik, Kurt, Parmigiani, Giovanni (Ed.), Use R! Springer-Verlag, New York, pp. VIII, 213.

Wickler, W., Seibt, U., 1980. Vocal Dueting and the Pair Bond II. Unisono dueting of the African forest weaver, Symplectes bicolor. Zeitschrift für Tierpsychologie 52, 217-226.

Wild, J.M., 2004. Functional Neuroanatomy of the Sensorimotor Control of Singing. Annals of the New York Academy of Sciences 1016, 438-462.

Wilson, S., Qi, J., Filipp, F.V., 2016. Refinement of the androgen response element based on ChIP-Seq in androgen-insensitive and androgen-responsive prostate cancer cell lines. Scientific Reports 6, 32611.

Wingfield, J.C., Smith, J.P., Farner, D.S., 1982. Endocrine Responses of White-Crowned Sparrows to Environmental Stress. The Condor 84, 399-409.

Yates, A., Akanni, W., Amode, M.R., Barrell, D., Billis, K., Carvalho-Silva, D., Cummins, C., Clapham, P., Fitzgerald, S., Gil, L., Girón, C.G., Gordon, L., Hourlier, T., Hunt, S.E., Janacek, S.H., Johnson, N., Juettemann, T., Keenan, S., Lavidas, I., Martin, F.J., Maurel, T., McLaren, W., Murphy, D.N., Nag, R., Nuhn, M., Parker, A., Patricio, M., Pignatelli, M., Rahtz, M., Riat, H.S., Sheppard, D., Taylor, K., Thormann, A., Vullo, A., Wilder, S.P., Zadissa, A., Birney, E., Harrow, J., Muffato, M., Perry, E., Ruffier, M., Spudich, G., Trevanion, S.J., Cunningham, F., Aken, B.L., Zerbino, D.R., Flicek, P., 2016. Ensembl 2016. Nucleic Acids Research 44, D710-D716.

Yu, A.C., Margoliash, D., 1996. Temporal hierarchical control of singing in birds. Science 273, 1871-1875.

Zembrzycki, A., Griesel, G., Stoykova, A., Mansouri, A., 2007. Genetic interplay between the transcription factors Sp8 and Emx2 in the patterning of the forebrain. Neural Development 2, 8.

Zhang, W., Guo, Y., Li, J., Huang, L., Kazitsa, E.G., Wu, H., 2016. Transcriptome analysis reveals the genetic basis underlying the seasonal development of keratinized nuptial spines in Leptobrachium boringii. BMC Genomics 17, 978.

Zhao, W., Yuan, T., Fu, Y., Niu, D., Chen, W., Chen, L., Lu, L., 2021. Seasonal differences in the transcriptome profile of the Zhedong white goose (Anser cygnoides) pituitary gland. Poult Sci 100, 1154-1166.

Zornik, E., Kelley, D.B., 2011. A neuroendocrine basis for the hierarchical control of frog courtship vocalizations. Front Neuroendocrinol 32, 353-366.

Tables

Table 1. Experimental groups and sample sizes.

				Sample size (n)				
Group	Sex	Singing	Tissue sampled	Song analysis	Body weight, brain weight, Plasma androgens	HVC volume	Microarray	Oviduct weight
CON	Female	No	HVC	-	6	6	5	6
T1h	Female	No	HVC	-	6	6	6	2
T3h	Female	No	HVC	-	6	6	5	2
T8h	Female	No	HVC	-	6	6	5	6
T3d	Female	No	HVC	-	6	5	6	3
T7d	Female	Yes	HVC	5	6	6	6	6
T14d	Female	Yes	HVC	6	6	6	6	6

CON: control birds treated with empty implants; HVC: used as a proper name. Testosterone treatments: 1 hour (h) [T1h], 3 h [T3h], 8 h [T8h], 3 days (d) [T3d], 7 d [T7d], and 14 d [T14d].

Supplementary Figures and Legends

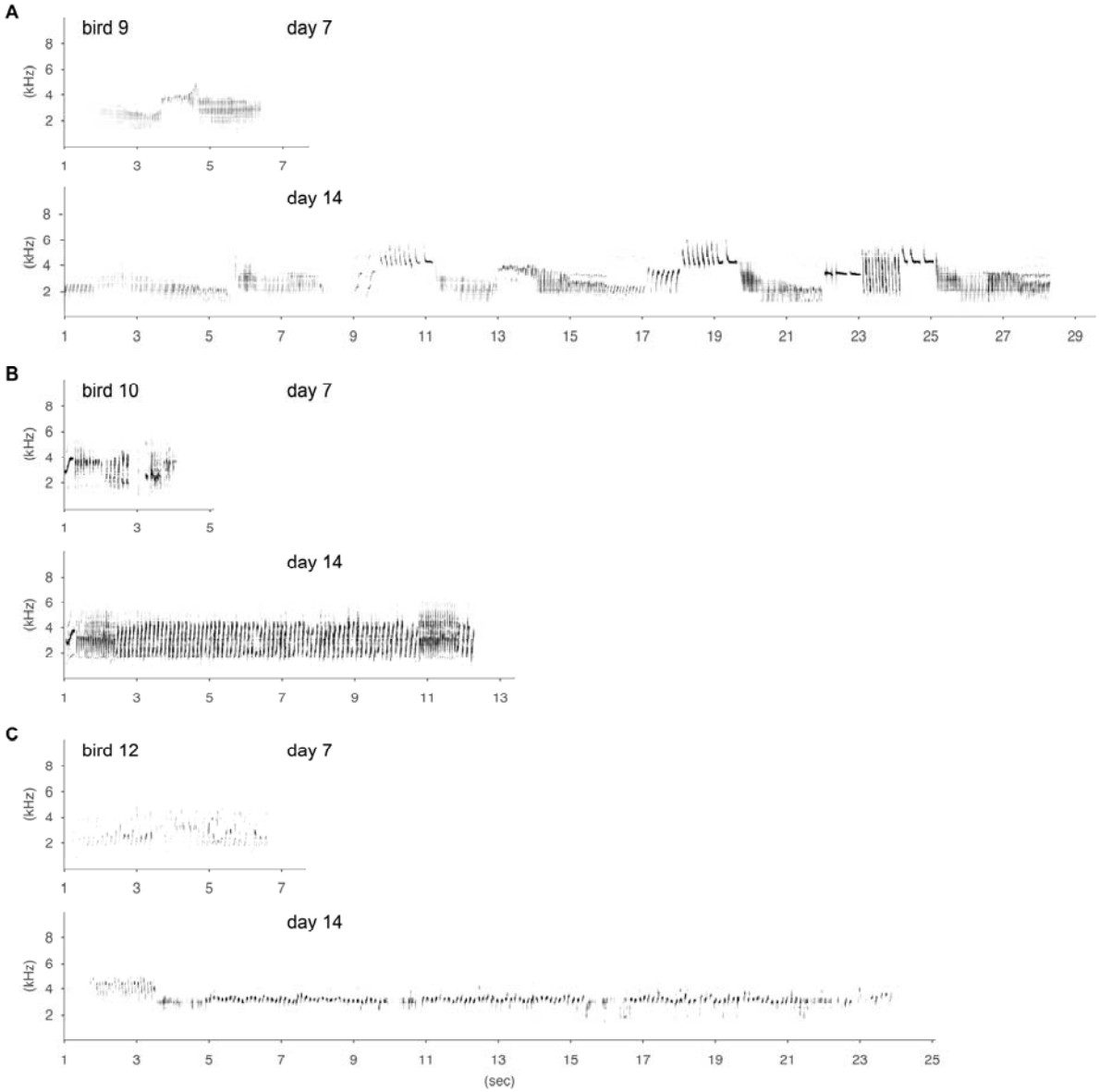

Figure 1 – Figure supplement 1. Representative song spectrograms of the song development of three T14d birds. Note that the song length, syllable repetitions, and amplitude (the intensity of the spectrogram) of the three birds increased over time. Bird 9 developed the most male-typical song patterns.

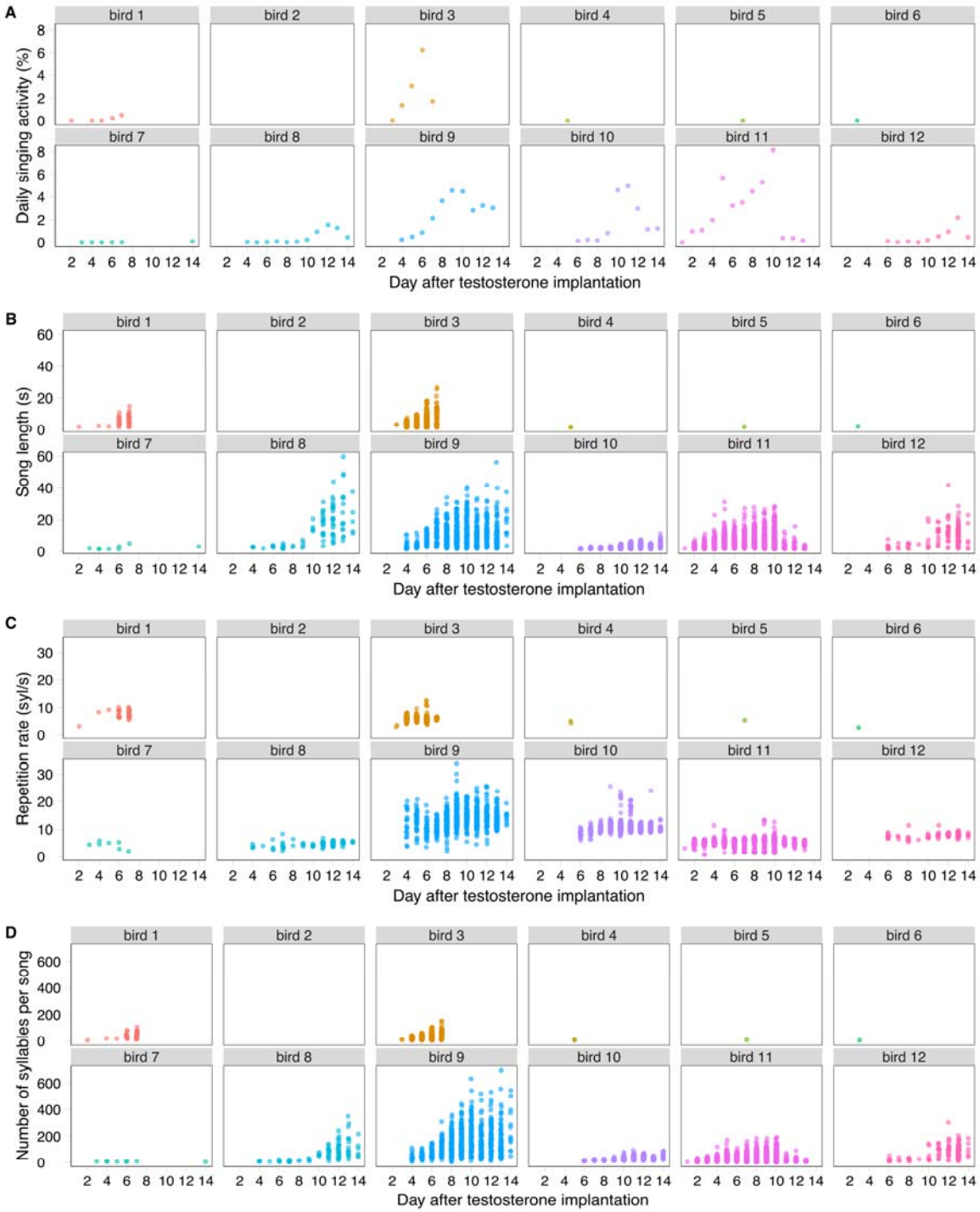

Figure 1 – Figure supplement 2. Inter- and intra-individual variability of daily singing activity (A), song length (B), syllable repetition rate (C) and number of syllables per song (D) during song development. Each dot represents a measurement of a day in A and represents a song in B-D. Bird 1 to 6 belong to T7d and bird 7 to 12 belongs to T14d.

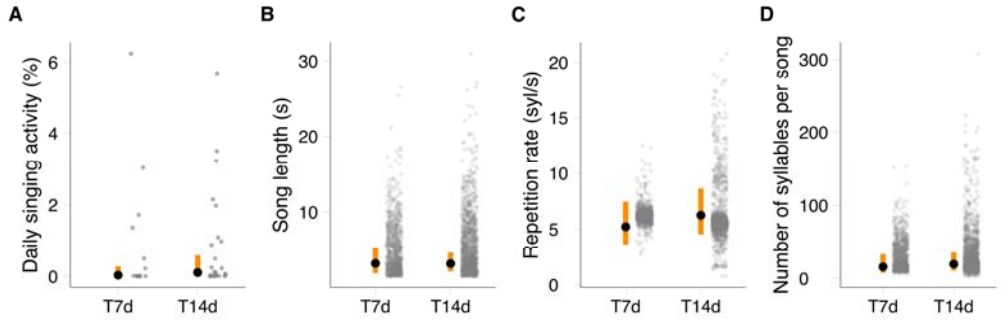

Figure 1 – Figure supplement 3. Song parameters quantified during the first seven days after testosterone implantation of female canaries. A, Daily singing activity as measured by the percentage of time spent singing within nine hours per day; **B**, song length in seconds (s); **C**, syllable repetition rate in syllables per second (sys/s); **D**, number of syllables in a song. Each gray dot represents the value per day of a bird in the T7d and T14d groups from day 1 to day 7 after testosterone implantation. The black dots indicate the predicted estimates of the linear mixed-effects models, and the vertical orange bars indicate the 95% credibility intervals (CrI) of the predicted estimates. There are no statistical differences between birds in these two groups, as can be seen from the overlapping 95% CRIs. See also Supplemental Table 2 and Supplemental Table 3 for the linear mixed-effect model estimates and posterior probability.

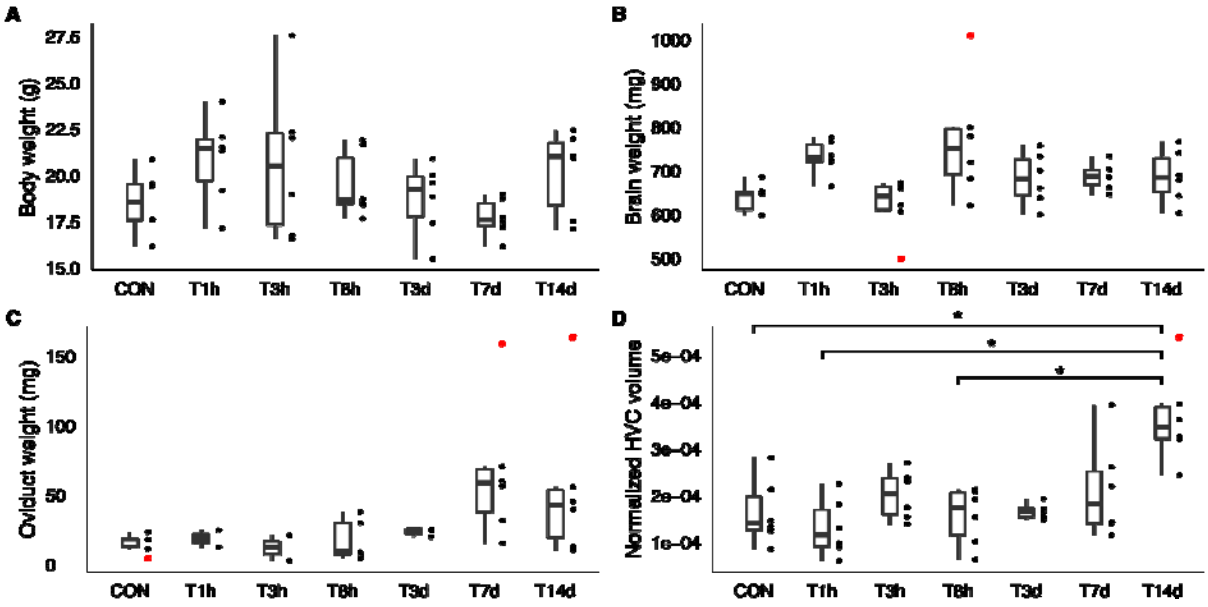

Figure 1 – Figure supplement 4. Physiological measurements of testosterone-implanted female canaries. A, no significant differences between control and testosterone-implanted groups in body weight (Kruskal-Wallis rank sum test, χ^2 = 7.47, df = 6, P-value = 0.28). **B**, Significant differences between control and testosterone-implanted groups in brain weight (Kruskal-Wallis rank sum test, χ^2 = 15.70, df = 6, P-value = 0.015. However, Dunn's post hoc test did not detected significantly differences in any pairs after P-value adjusted by Holm's method. **C**, no significant differences between control and testosterone-implanted groups in oviduct weight (Kruskal-Wallis rank sum test, χ^2 = 11.58, df = 6, P-value = 0.072). **D**, normalized HVC volume (against brain weight) of T14d were significantly different from that of control (CON), T1h, and T8h groups (Kruskal-Wallis rank sum test, χ^2 = 17.32, df = 6, P-value = 0.0082; Holm-adjusted P-value: CON vs. T14d 0.044; T1h vs. T14d 0.0043; T8h vs. T14d 0.046). The boxes indicate the $25^{th}/50^{th}/75^{th}$ percentiles (bottom/middle/top bar), and the extent of the whiskers indicates the most extreme values that are within 1.5 times of the inter-quartile range (IQR) of the hinge. Outliers are labeled in red. *: Holm-adjusted P-value <0.05 (Kruskal-Wallis rank sum test followed by Dunn's post hoc test using the "Holm" method).

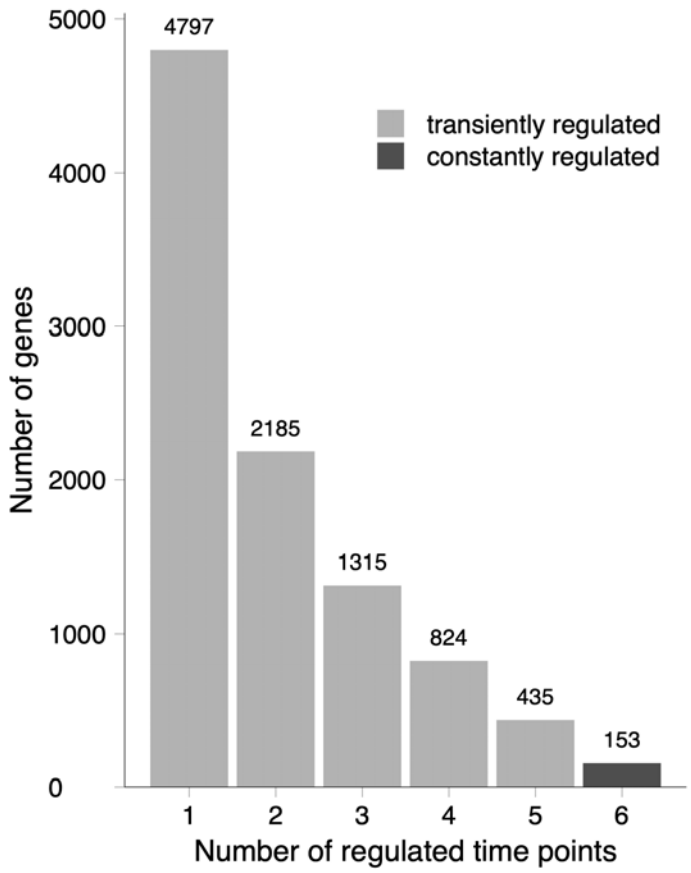

Figure 2 – Figure supplement 1. Dissecting transiently regulated genes by number of differentially regulated time points. The distribution of genes categorized as transiently regulated (light grey), based on the number of time points at which they are differentially expressed. Each bar represents the number of genes that are differentially expressed at one, two, or more time points, providing a more detailed view of the transiently regulated gene expression patterns.

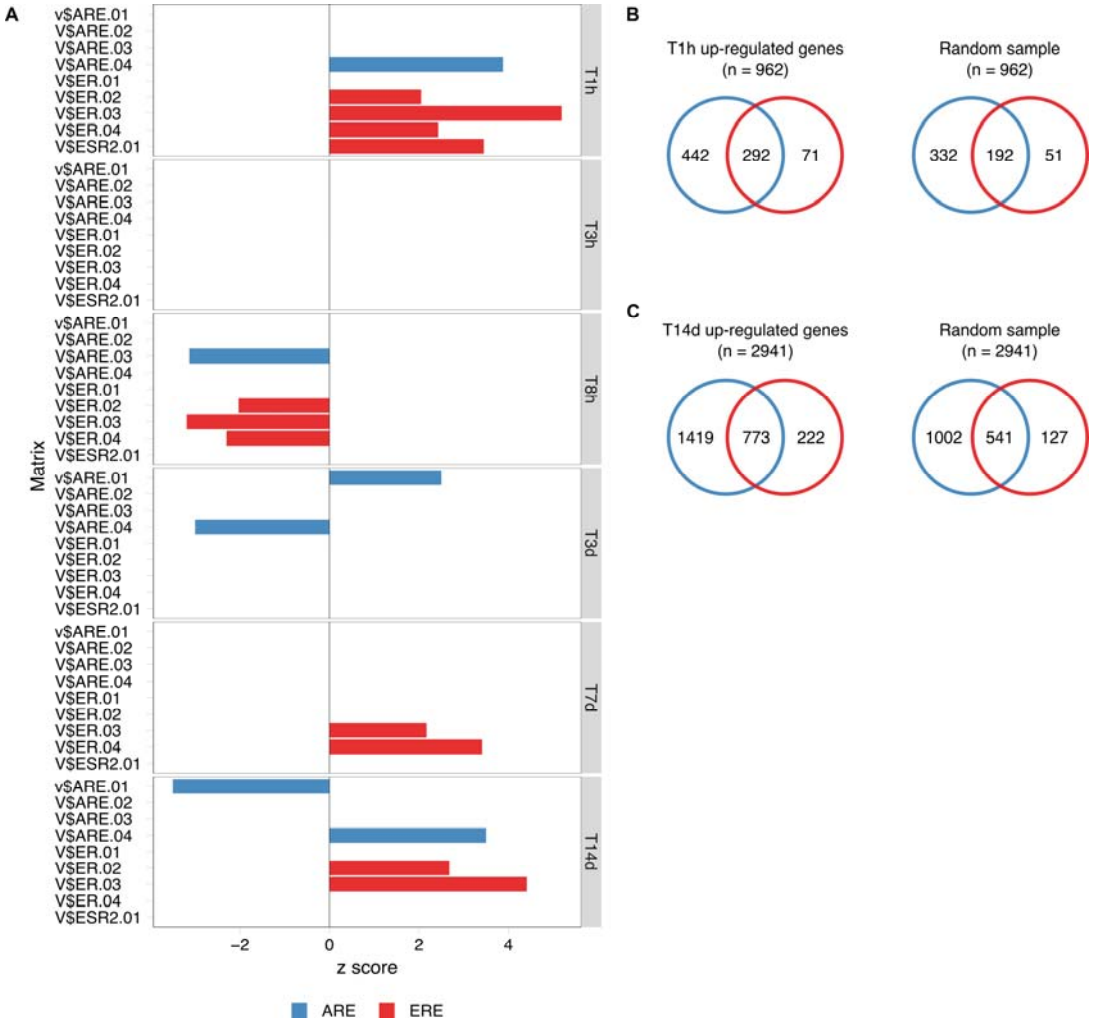

Figure 2 – Figure supplement 2. Over-representation of AREs and EREs in the promoter sequences of testosterone up-regulated genes. A, Z-scores of overrepresentation against the matching numbers of randomly sampled promoter sequences as the user-defined background (see also Supplemental Table 5). **B and C**, the number of promoter sequences having AREs (blue) or EREs (red) or both elements (intersect) of T1h up-regulated genes (B) or T14d up-regulated genes and their random samples, respectively.

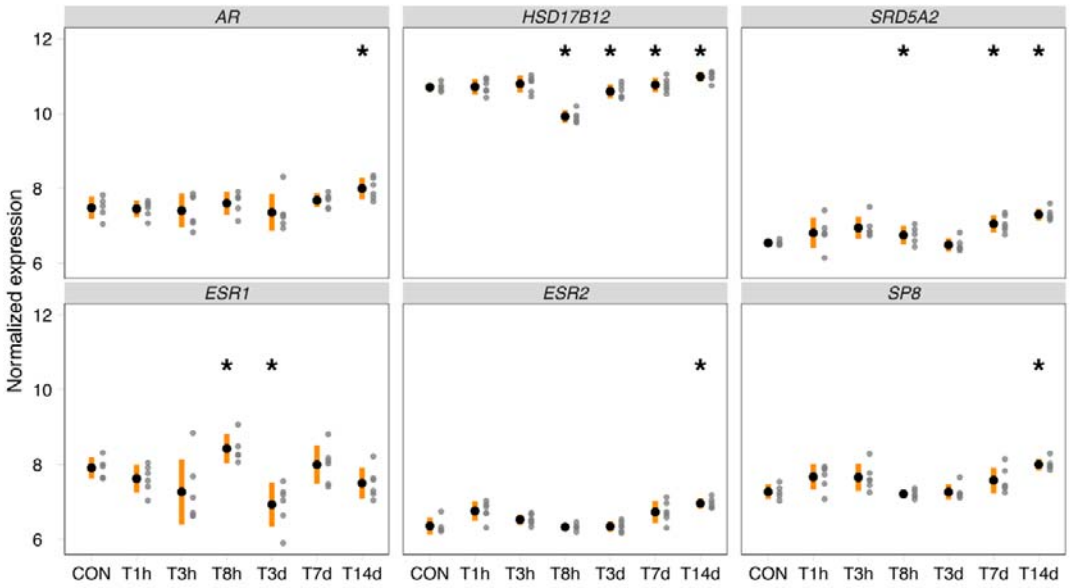

Figure 3 – Figure supplement 1. RMA normalized expression levels of selected genes. Each gray dot represents the RMA-normalized expression level for an individual bird. Black dots indicate the average expression levels, while vertical orange bars represent the standard deviation of these levels. Asterisks indicate genes that are significantly differentially expressed relative to the control group. The genes shown are: *AR*: androgen receptor; *HSD17B12*: 17β-hydroxysteroid dehydrogenase; *SRD5A2*: 5α-reductase 2; *ESR1*: estrogen receptor α; *ESR2*: estrogen receptor ß; *SP8*: Sp8 transcription factor.

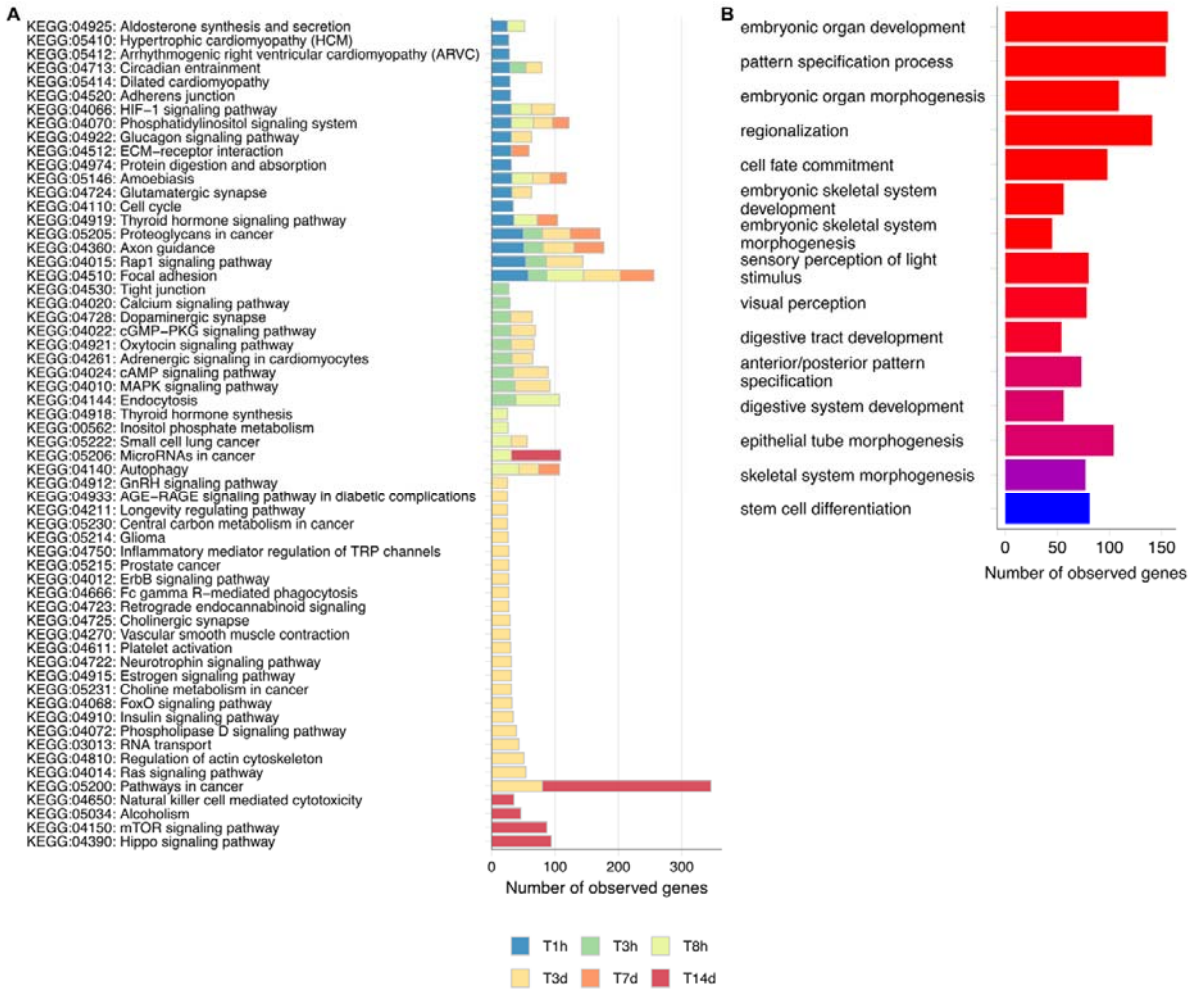

Figure 3 – Figure supplement 2. KEGG pathway and GO term enrichment analysis of differentially expressed genes during progressive testosterone action on HVC.

A, KEGG pathway enrichment analysis of differentially expressed genes at each time point. The number of observed genes (cumulative across time points) is presented in a stacked bar graph. The enriched KEGG pathways (based on Bonferroni-adjusted p-values) are displayed for each time point. Similar to GO term enrichment analysis results, testosterone seems to activate smaller-scale changes, such as focal adhesion, at early time points, while activating system-level pathways like the Hippo signaling pathway, which regulates organ size, at T14d. **B,** GO term enrichment analysis focusing on genes only differentially expressed at T14d, which shows primarily system-level biological processes. The figure shows the ten most probable GO terms based on Bonferroni-adjusted P-values.

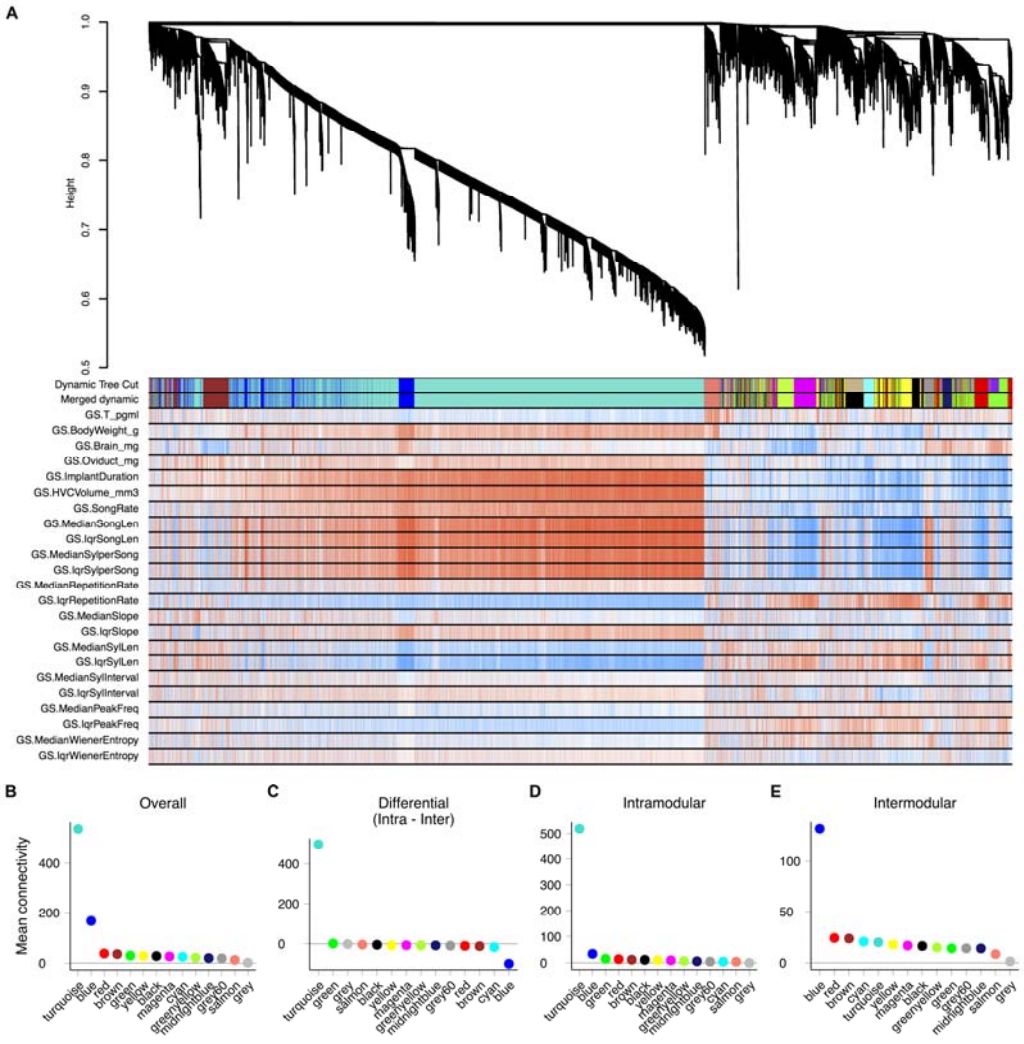

Figure 4 – Figure supplement 1. The unsupervised clustering method WGCNA classified differentially expressed genes into coexpression modules and grouped similar modules into 14 modules. A, WGCNA calculated the gene significance (GS) between the expression level of each gene and physiological traits (plasma androgen level (T), body weight, brain weight, oviduct weight, and HVC volume) and song measurements (song rate, song length, syllables per song, syllable repetition rate, syllable slope, syllable length, syllable interval, maximum frequency, entropy) by calculating the Pearson correlation matrix. Genes with positive gene significance are shown in red, while genes with negative are shown in blue. Iqr: inter-quartile range. Modules ranked by **B**, overall **C**, differential, **D**, intramodular, and **E**, intermodular connectivity. A module with high differential connectivity indicates that genes are more densely connected within the module than with the genes from other modules.

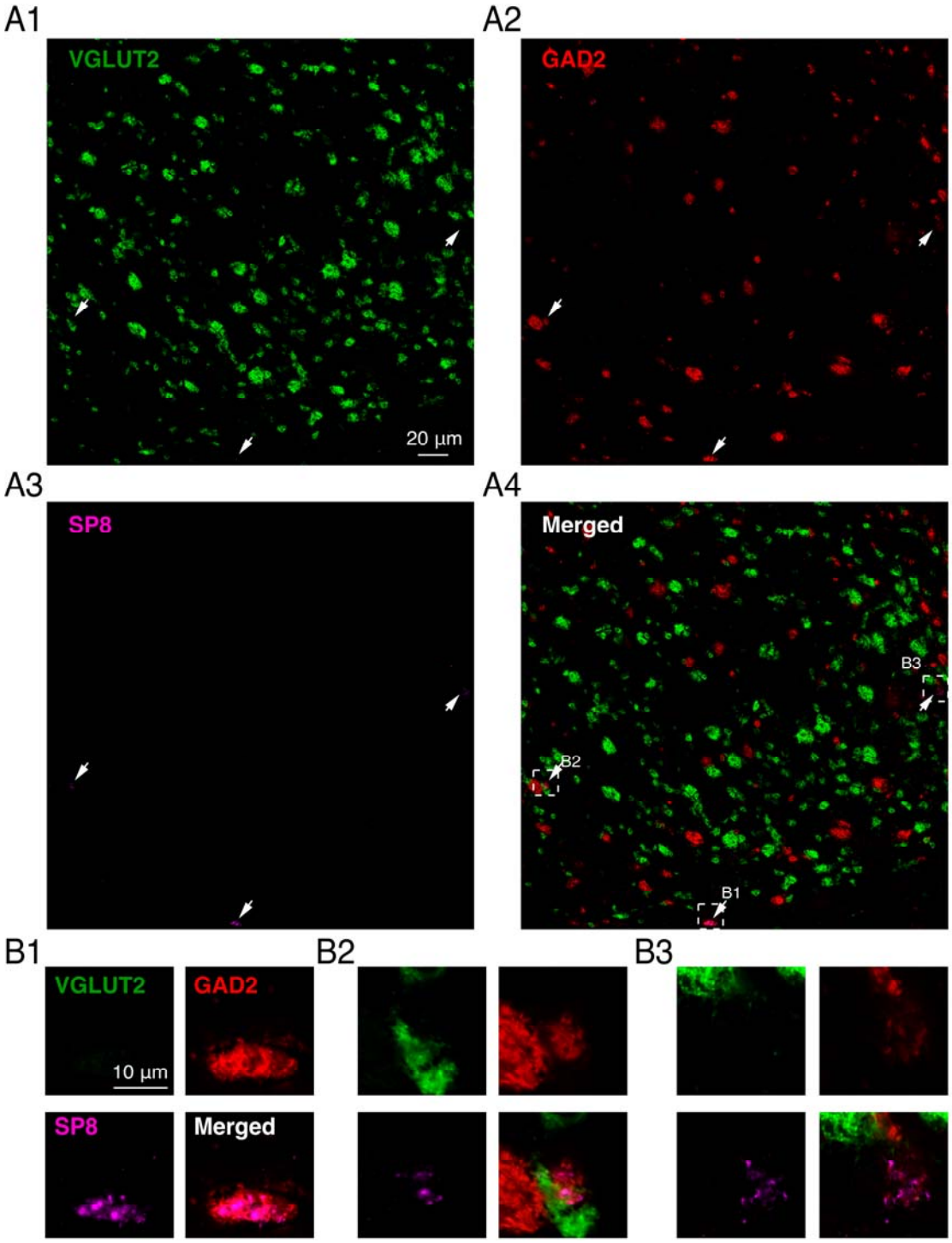

Figure 5 – Figure supplement 1. Expression of *SP8* in *GAD2* mRNA positive (GABAergic) cells in HVC. A, Representative images of RNAScope in situ hybridizations targeting *VGLUT2* (as also known as *SLC17A6*) (**A1**), *GAD2* (**A2**) and *SP8* (**A3**) mRNAs, merged in (**A4**). Single confocal planes are shown. Arrows indicate three *SP8* and *GAD*2 mRNA coexpressing cells, which are *VGLUT2* mRNA-negative, enlarged in **B1**, **B2** and **B3**.

Supplementary Files and Legends.

Supplementary File 1. Summary table for measured song parameters (mean ± SD).

Supplementary File 2. Estimates of fixed and random effects of linear mixed effect models. We present fixed (β) and random (σ2) parameters with their 95% credible intervals (CrI). A statistically meaningful effect of a fixed factor can be assumed if zero is not included within the 95% CrI, and was labeled with *.

Supplementary File 3. The posterior probability of a mean difference between compared factors of linear mixed effect models. Comparisons with statistically meaningful differences, defined by posterior probability > 0.95, were indicated with ***.**

Supplementary File 4. List of differentially expressed genes. The output of the differential analysis performed using ChipInspector software. Additional power analysis was performed as described in the methods section "Analysis of differentially expressed genes" of the manuscript.

Supplementary File 5. List of constantly regulated genes.

Supplementary File 6. Over-representation of AREs and EREs in the promoter sequences of testosterone up-regulated genes. Reported values are Z-scores of overrepresentation against the matching numbers of randomly sampled promoter sequences as the user-defined background.

Supplementary File 7. MatInspector identified AREs and EREs in the promoter sequences of T1h up-regulated transcription factors.

Supplementary File 8. GO-term enrichment analysis of differentially expressed genes of each time point.

Supplementary File 9. Enrichment analysis of search terms using Fisher's exact test. P-values were corrected using the "FDR" method.

Supplementary File 10. Expression levels of genes associated with particular cell types.

Supplementary File 11. Connectivity and gene significance of genes assigned to the "turquoise" module by WGCNA. Overall connectivity (kTotal); Intramodular connectivity (kWithin); Intermodular connectivity (kOut); Differential connectivity (kDiff). GS: gene significance.

Supplementary File 12. List of genes (625) contains SP8 binding sites in proximal promoter sequences.

Supplementary File 13. List of genes (169) contains SP8 and GATA binding sites in proximal promoter sequences.

Supplementary File 14. List of RNAScope probes used in this study.